Final Draft
of the original manuscript:

Floeter, J.; Beusekom, J.E.E.van; Auch, D.; Callies, U.; Carpenter, J.; Dudeck, T.; Eberle, S.; Eckhardt, A.; Gloe, D.; Haenselmann, K.; Hufnagl, M.; Janssen, S.; Lenhart, H.; Moeller, K.O.; North, R.P.; Pohlmann, T.; Riethmueller, R.; Schulz, S.; Spreizenbarth, S.; Temming, A.; Walter, B.; Zielinski, O.; Moellmann, C.:

Pelagic effects of offshore wind farm foundations in the stratified North Sea

In: Progress in Oceanography (2017) Elsevier

DOI: 10.1016/j.pocean.2017.07.003

Pelagic effects of offshore wind farm foundations in the stratified North Sea

Jens Floeter*, Justus E. E. van Beusekom**, Dominik Auch*, Ulrich Callies**, Jeffrey Carpenter**, Tim Dudeck*, Sabine Eberle*, André Eckhardt*, Dominik Gloe*, Kristin Hänselmann*, Marc Hufnagl*, Silke Janßen*, Hermann Lenhart+++, Klas Ove Möller**, Ryan P. North++, Thomas Pohlmann++, Rolf Riethmüller**, Sabrina Schulz*, Stefan Spreizenbarth*, Axel Temming*, Bettina Walter*, Oliver Zielinski+, Christian Möllmann*

*) Institut für Hydrobiologie & Fischereiwissenschaft, Universität Hamburg, Grosse Elbstrasse 133, D-22767 Hamburg

**) Helmholtz-Zentrum Geesthacht, Zentrum für Material- und Küstenforschung GmbH, Max-Planck-Str. 1, D-21502 Geesthacht

+) Institute for Chemistry and Biology of the Marine Environment, University of Oldenburg, Schleusenstr. 1, 26382 Wilhelmshaven

++) Institut für Meereskunde, Universität Hamburg, Bundesstrasse 53, D-20146 Hamburg,

+++) Research Group Scientific Computing, Universität Hamburg, Bundesstraße 45a, D-20146 Hamburg

Corresponding author:

Jens Floeter
Institut für Hydrobiologie & Fischereiwissenschaft,
Universität Hamburg, Olbersweg 24,
D-22767 Hamburg
Phone +49 (0)40 42838 6622
Fax +49 (0)40 42838 6618
e-mail: jfloeter@uni-hamburg.de

Abstract

A recent increase in the construction of Offshore Wind Farms (OWFs) has initiated numerous environmental impact assessments and monitoring programs. These focus on sea mammals, seabirds, benthos or demersal fish, but generally ignore any potential effects OWFs may have on the pelagic ecosystem. The only work on the latter has been through modelling analyses, which predict localised impacts like enhanced vertical mixing leading to a decrease in seasonal stratification, as well as shelf-wide changes of tidal amplitudes. Here we provide for the first-time empirical bio-physical data from an OWF. The data were obtained by towing a remotely operated vehicle (TRIAXUS ROTV) through two non-operating OWFs in the summer stratified North Sea. The undulating TRIAXUS transects provided high-resolution CTD data accompanied by oxygen and chlorophyll-*a* measurements. We provide empirical evidence that vertical mixing is increased within the OWFs, leading to a doming of the thermocline and a subsequent transport of nutrients into the surface mixed layer (SML). Nutrients were taken up rapidly because underwater photosynthetically active radiation (PAR) enabled net primary production in the entire water column, especially within submesoscale chlorophyll-*a* pillars that were observed at regular intervals within the OWF regions. Video Plankton Recorder (VPR) images revealed distinct meroplankton distribution patterns in a copepod-dominated plankton community. Hydroacoustic records did not show any OWF effects on the distribution of pelagic fish. Our survey results are compared with measurements from pre-OWF times and found to fit into the corridor of natural variability.

Highlights

- First time bio-physical empirical evidence of OWF effects on the pelagic ecosystem
- High speed, high-resolution remotely operated vehicle (TRIAXUS ROTV) transects
- We provide evidence for increased vertical mixing within the OWFs
- There was doming of the thermocline and vertical nutrient transport within the OWFs
- Submesoscale chlorophyll-*a* pillars occurred at regular intervals

Keywords

Offshore Wind Farms, TRIAXUS ROTV, offshore structures, pelagic environment, chlorophylls, North Sea

Introduction

In 2015 offshore wind power installations represented 24% of the annual EU wind energy market, and the number of new installations continues to increase (Corbetta et al., 2016). As of the summer of 2016 a total of 3,344 offshore wind turbines in 82 wind farms across 11 European countries were fully connected to the grid, providing a combined capacity of 11,538 MW (Pineda and Ruby, 2016). The German strategic goal of 80% renewable energy supply by 2050 is partly based on the production of offshore wind energy within the German Exclusive Economic Zone (EEZ (EEG, 2014)). Germany has the largest installed wind power capacity (45 GW) in the EU, and installed 6 GW in 2015 alone, of which 38% were offshore (Corbetta et al., 2016). In the German EEZ 18 wind farm projects with a total of 1,285 turbine foundations are either approved, in operation or under construction (BSH, 2015). The EEG 2014 objective of an installed offshore wind power capacity of 15 GW in 2030 will lead to a further advance of offshore wind farm (OWF) development at greater distances from the coast to mitigate environmental impacts and changes in the characteristic landscape.

As part of the approval procedure for OWFs in the German EEZ, potential adverse impacts of the planned facilities on the marine environment have to be assessed through an Environmental Impact Assessment (EIA). The German EIA standard (StUK4; BSH, 2013) only considers ecosystem components that have conservation relevance, i.e. demersal fish, benthos, birds, and marine mammals. The investigation or monitoring of the potential effects of OWFs on the pelagic ecosystem is not required. Thus, only a limited number of studies have analysed OWF effects on the pelagic ecosystem, and even fewer include field measurements. One such study, at the OWF alpha ventus (45 km off the coast at a water depth < 30 m), measured oceanographic parameters and currents at a fixed station; the distribution of pelagic fish was also monitored with a horizontally oriented hydroacoustic system (Krägefsky, 2014). The observations revealed that during August 2007 pelagic fish, most likely mackerel, had their highest abundances within 100 m of underwater construction sites (Schröder et al., 2013).

Most other studies have been analytical and modelling studies, whose results suggest OWFs induce changes in vertical water column dynamics and subsequently key biological processes. In one of the first studies on OWF impacts on upper ocean hydrography, Broström (2008) analytically showed that the extraction of energy from the wind creates an upwelling / downwelling dipole in the surface mixed layer through divergence in the Ekman transport. Broström (2008) concluded that water surface wind stresses at wind speed of 5 - 10 ms^{-1} may generate vertical water velocities exceeding 1 $mday^{-1}$ and that the generated upwelling is able to affect the ambient ecosystem. Nerge and Lenhart (2010) simulated an artificial OWF within a three-dimensional model of shelf sea dynamics (Backhaus, 1985; Pohlmann, 1996, 2006). They confirmed the creation of an upwelling / downwelling dipole using a more realistic meteorological forcing and concluded that an OWF could have the potential to alter the seasonal development of tidal fronts, but they did not consider subsequent ecological impacts. Field measurements to assess potential OWF impacts on nutrient dynamics, plankton distribution and production have not yet been conducted. Paskyabi et al. (2012) showed that the dipoles are sensitive to wind stress, wave forcing and the size of the OWF, and have a tendency to become asymmetric with time. Simulations showed that the winds and wind-driven waves passing a large OWF generate downstream eddies of a similar size as the OWF and their time scale is up to several days (Paskyabi and Fer, 2012). Ludewig (2015) used a 3D hydrodynamic model with realistic atmospheric forcing to show that a small OWF with 12 turbines could affect the upper ocean dynamics within 100 km on the leeside and that the upwelling / downwelling cells could have a diameter of 15 km. In addition to wind-wake effects, underwater structures may impact the local hydrodynamics. Lass et al. (2008) measured enhanced mixing downstream of a pile in an estuarine flow in the Baltic Sea. While the simulations of Paskyabi et al. (2012) had eddies the size of an OWF, Lass et al. (2008) observed enhanced mixing and eddies with a characteristic diameter of the monopile and a frequency corresponding to a von Kármán vortex street. Rennau et al. (2012) applied a numerical model to assess monopile induced mixing in a dense bottom current, representative of the western Baltic Sea. They calculated an additional vertically integrated positive buoyancy production in an area on the order of 10 monopile diameters. However, the impact of structure-induced mixing due to realistic wind farm distributions was rather low, with a typical decrease in the bottom water salinity in the range of 0.1−0.3.

Most recently, Cazenave et al. (2016) applied a 3D unstructured grid model (FVCOM) to focus solely on the impact of the physical presence of the turbine monopiles. In a mixed or stratified eastern Irish Sea, the effects of 242 wind turbine monopiles from 7 OWFs were explicitly described within the tidal current regimes from January and May 2011. The spatial resolution increased from 2.5 m to 10 km with distance from the monopiles. A resulting 5% reduction of horizontal maximum current speed was found within a radius of 1 km, i.e., approximately 250 times the monopile diameter. Monopiles were found to increase local vertical mixing within a radius of only 200 m, but an OWF was found to have a 5-15% impact on stratification in May 2011, affecting an area approximately 80,000 times larger than the footprint of its 162 monopiles.

In contrast, Carpenter et al. (2016) concluded that OWFs are expected to have very little impact on large-scale stratification at the current capacity in the North Sea. Their study used order of magnitude estimates of mixing and advection time scales, and compared their results for water bodies with OWFs to natural stratification variability. However, if development continues as predicted, the impact of OWFs could become significant at the OWF scale and at the southern North Sea scale.

As concluded by Clark et al. (2014), observational studies on the bio-physical impacts of OWFs on the pelagic ecosystem are still missing, yet they are necessary to validate model results. Therefore, we provide for the first-time empirical results from a bio-physical survey of two OWFs in the North Sea during the summer stratification period. As a follow-up to previous theoretical and modeling investigations, the key objective of the survey was to provide initial empirical evidence of potential OWF foundation effects on:

1. ambient hydrography
2. local nutrient concentrations
3. light availability and primary production
4. zooplankton and pelagic fish distribution

A high-speed remotely operated towed vehicle (ROTV) TRIAXUS system was deployed to identify potential impacts of wind turbine foundations. As the OWFs were not operating, the results only consider the effects of the interactions of the foundations with tidal and wind driven currents. We covered an area within approx. 20 km of the OWFs and obtained high resolution abiotic and biotic data, including temperature, chlorophyll-a fluorescence, nutrients, and the abundance and distribution of plankton and pelagic fish. Particle drift modelling was conducted to hindcast the trajectories of the sampled water bodies and calculate OWF contact times. In addition, the observations were compared with model predictions and with hydrographic measurements conducted during a previous summer cruise, before the OWFs were built.

Material & Methods

Surveys

Field measurements were conducted during a summer cruise (HE429, July 19. - 24. 2014) with the RV Heincke. The two OWFs that were surveyed, Global Tech I (GTI) and BARD Offshore 1 (BARD), are located at a water depth of around 40 m in the German EEZ, and a distance of approx. 100 km offshore. Both OWFs had 80 wind power plants installed, GTI has tripod foundations and BARD has tripile foundations. The turbines were not in operation and the rotors were not turning, i.e., any observed effects are solely attributed to the foundations and changes in the wind field due to the static presence of the piles, turbines and rotors.
On the 14th of July 2010, two years before construction of the OWF GTI, the RV Heincke made a North-South ROTV transect through the area. The then recorded ScanFish ROTV data therefore provides a baseline to get indications of any potential OWF effects.

Satellite measurements

Moderate Resolution Imaging Spectroradiometer (MODIS) sea surface temperature (SST) data and chlorophyll-*a* concentrations originally obtained from ftp://podaac-ftp.jpl.nasa.gov/ were provided by the Integrated Climate Data Center (ICDC, icdc.cen.uni-hamburg.de) University of Hamburg, Hamburg, Germany. Only SST data from nightly overflights were used, with a spatial resolution of ~ 4 km. Due to extensive cloud coverage the only data that could be analysed was from the 23rd of July 2014.

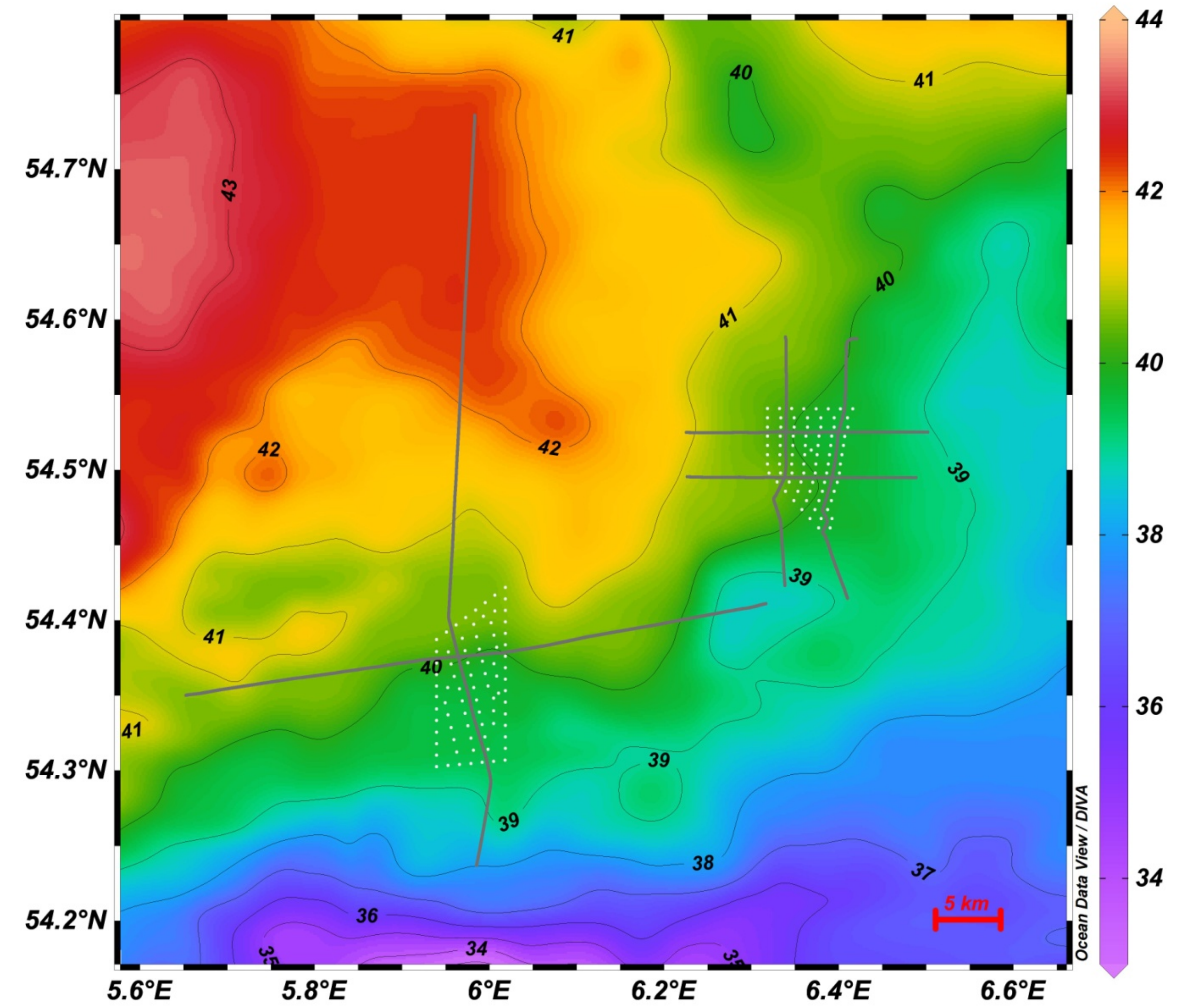

Figure 1: TRIAXUS transects (grey lines) in relation to the BARD and GTI wind turbines (white dots) overlaying colour contours of the local bathymetry [m] of the survey area.

Field measurements

High speed large scale measurements were conducted with a MacArtney TRIAXUS ROTV equipped with a pumped Seabird Fast Cat SBE 49 CTD, an AADI Oxygen Optode 4330F, a pumped Turner Designs C6 Multi-Sensor Platform (chlorophyll-*a*, phycocyanin, phycoerythrin, temperature), a Laser Optical Plankton Counter (LOPC, ODIM) and also with a Video Plankton Recorder (VPR, Seascan). Data were recorded at a frequency of 1 Hz and the ROTV was towed at a speed of 8 knots (4.1 ms^{-1}) with a three-degree lateral offset to lessen any disturbance from the vessels wake. During most transects (Fig. 1) the ROTV was undulating with a vertical speed of 0.1 ms^{-1} from ~ 4 m below the sea surface to ~ 8 m above the sea floor. This results in vertical data spacing of 0.3 m and a horizontal resolution of around 560 m between two surface undulation turning points. For two transects the ROTV was towed at a constant depth of 13 m. Photosynthetically active radiation (PAR, 400-700 nm)) was recorded every 5 s with a TriOS Ramses-ACC irradiance sensor mounted on the TRIAXUS and calculated according to Kirk (1994). Global radiation (GR) was recorded every 60 s on the upper deck of the research vessel using the secondary standard pyranometer Kipp & Zonen CMP 11.

Light availability is a major factor in phytoplankton growth in the euphotic zone, which is limited by the 1% depth (z) of PAR (z_1%_PAR) as its lower boundary. Based on the measured PAR(z) values along each upward single profile we calculated the diffuse attenuation coefficient Kd through linear regression of the log-transformed PAR(z) profile and then estimated z_1%_PAR as 4,605/Kd (Kirk, 1994). It is expected that the 1% PAR depth is slightly overestimated with this approach (< 5%, i.e., the true depth is ~1.0 - 1.5 m shallower), since the high absorption of red wavelengths in the upper ~4 meters of the water column is not measured by the undulating radiometer (Zielinski et al. 2002).

Stationary vertical hydrographic profiles were taken from the downcasts of a Seabird SBE 911plus CTD. Water samples for nutrient analyses were taken at 3 depths (5 m, centre of thermocline, 5 m above seafloor) during the CTD upcast using a Hydro-Bios Freeflow (12 x 4 l) carousel water sampler. Before closure the bottles were kept at the sampling depth for 2 minutes to ensure complete flushing with ambient water. Chlorophyll-*a* fluorescence was measured during the CTD downcast using a calibrated WETlabs ECO FL(RT) Chlorophyll-*a* sensor and subsequently used to calibrate the relative chlorophyll-*a* fluorescence measurements of the ROTV. Water samples were filtered through 0.45 µm in-line filters attached to a 60 ml syringe, frozen at -80 °C and stored on land at -20 °C. After thawing, nutrients (NO, NO3, NO2, Si, PO4, NH4) were analyzed with a Seal Analytical Autoanalyser AA3 using a fluorescence based method for NH4 (based on Kerouel and Aminot, 1997) and spectrophotometric methods for all other constituents (based on Grasshoff et al., 1983).

Plankton images were recorded at 25 image-frames per second with a VPR (Möller et al. 2012, 2015). Plankton densities were calculated by taking the calibrated image volume of a single frame into account. A two-step taxonomic identification was performed as the automatic classification results (Hu and Davis, 2006) were manually controlled and corrected afterwards. The 15 classification groups were: appendicularia, bipinnaria, cladocera, copepoda, decapoda, dinoflagellata, gastropoda, gelatinous plankton, marine snow, nauplii, ophiuroida, pilidium, pluteus, polychaeta, rodshaped plankton (see appendix for a selection of example images).

For ground-truthing of the VPR images, a total of 19 zooplankton WP2 net (57 cm diameter, 150 µm mesh size, heave speed 0.3 m/s) samples were obtained from vertical hauls integrating from 2 m above the seafloor to the sea surface. Taxonomic compositions were quantified using a ZooScan (Gorsky et al., 2010; version 2). We used ImageJ software (version 1.41o) with ZooProcess (version 7.19) and Plankton Identifier software (Gasparini and Antajan, 2013; version 1.3.4) for image analysis and automatic plankton identification, but all images were manually controlled and corrected afterwards.

During steaming and ROTV towing with at least 8 kn (4.1 ms^{-1}) and only between 04:30 a.m. and 06:30 p.m. (UTC) hydroacoustic measurements were recorded with four hull mounted Simrad EK60 transducers (38, 70, 120, 200 KHz). Pelagic fish schools were identified using Echoview 4.9 (Myriax) and nautical area scattering coefficients (NASC, $\geq$ 0, [$m^2 nmi^{-2}$]) were calculated with an integration threshold of -55 dB and a resolution of one nautical mile (nmi).

During the July 2010 pre-OWF survey with RV Heincke (HE331) a ScanFish Mark III (EIVA) ROTV was towed with a speed of approximately 8 kn from North to South through the area in which the construction of the OWF Global Tech I started in 2012. The ScanFish is an undulating high speed ROTV sensor platform, similar to the TRIAXUS ROTV, except that it cannot be laterally shifted. The ScanFish was equipped with a CTD (conductivity: ADM

Elektronik, Germany; water temperature: PT100, ADM Elektronik, Germany; pressure: PA-7, Keller AG, Switzerland,) and a Chlorophyll-a fluorescence sensor (TriOS MicroFlu-chl, TRIOS Inc., Germany). Data were recorded at 11 Hz while undulating from 3 m below the sea surface to 3 m above the seafloor. This results in vertical data spacing of 0.04 m and a horizontal resolution of around 550 m between two surface undulation turning points. Conductivity and water temperature sensors were calibrated against reference standards directly before and after the ship survey.

Data Analysis

Data analysis and visualization was conducted using the software program R (R Core Team, 2015), the R-package "plyr" by Wickham (2011), Ocean Data View 4.78 (ODV, Schlitzer, 2016), Matlab R2015a and ESRI ArcMap® (10.3.1). Hydroacoustic data were gridded using the R “raster” package of Hijmans and van Etten (2012). Data were gridded using the ODV weighted average or ODV/DIVA method with automatic scale lengths (Troupin et al., 2012). We used the cmocean colour maps within ODV following the guidelines of Thyng et al. (2016).

Stratification index

The stratification indices for the TRIAXUS transects were derived from the two-dimensional ODV/DIVA estimations (Schlitzer, 2015, Troupin et al., 2012) of the potential density anomaly. The calculation follows the approach of Simpson (1981) by considering changes in the potential energy relative to the mixed condition (eq. 2 in Simpson, 1981). Due to the restricted depth range of profiling (4 to 30 m for BARD and 4 to 25 m for GTI), water densities in the upper and lower mixed layers were linearly extrapolated to the surface and a bottom depth of 40 m. This enabled comparisons between transects with a different profiling range, and ensures an accurate quantification of the degree of stratification that can be compared to previous studies and estimates (e.g., Carpenter et al., 2016). A lower stratification index indicates that less energy is needed to completely mix the water column.

Water currents

The regional meteorologically and tidally driven currents during the survey period were obtained from the baroclinic 3-D ocean circulation model BSHcmod with a horizontal resolution of ~ 5 km and an output time step of 15 minutes (Dick et al., 2001). The modelled current data were used to identify the up-, and downstream sides of the OWFs during our measurement periods.

Daily averages of vertically integrated residual currents were obtained from the 2-D version of the hydrodynamic circulation model TRIM (Casulli and Stelling, 1998). The model was parallelized and run in a nested mode with three refinements (Kapitza, 2008); the finest resolution was 1.6 km in the German Bight. Based on existing long-term simulations (Gaslikova, 2013, later extended), Callies et al. (2016) conducted a Principal Component Analysis (PCA) to characterize changes in the typical ambient current regimes in terms of only a few daily PC values covering the period Jan 1958 – Aug 2015. Short term data related to the present field campaign were extracted from this long-time series.

Particle drift modelling

Previous drift routes of water masses sampled with the vertically deployed CTD / water sampler were estimated using the particle tracking model PELETS (Callies et al., 2011). Passive tracer particles released at the time and location of sampling were transported 10 days backward in time, based on 2-D (i.e. vertically averaged) hydrodynamic currents from TRIM (see above). Spatial positions were recorded every hour, from which the total time that each particle spent within an OWF was back-calculated. This calculation was limited to the 10 days leading up to time the measurement was taken.

Results

Water currents

The currents in the German Bight are predominantly driven by tides and meteorological forcing. During the surveys the wind was at first blowing from the southeast, but switched on July 21th to a north-easterly direction. The average wind direction was 70° (cv = 61%) and the average speed was 6.5 ms^{-1} (cv = 37%, see appendix for a wind time series plot).

During the survey maximum ambient currents were on the order of 0.5 ms^{-1}. During the longitudinal TRIAXUS transects through GTI the current direction was stable from East to West for 2 - 5 hours (i.e., the upstream side to the East; Tab. 1). Shortly before the start of the horizontal North - South transect through GTI the tide turned, so that the currents were from West to East (i.e., upstream side to the West). The tide changed during the longitudinal TRIAXUS transect through BARD: the current was West to East for the first ~ 5 hours, then reversed. The following day approximately half-way through the BARD North - South transect the tide changed back to East to West (see appendix for details).

Table 1: Description of the ambient current fields during the TRIAXUS transects in relation to the OWFs.

	Current		OWF	
TRIAXUS transect	**Speed [m s^{-1}]**	**Direction [°]**	**Upstream**	**Downstream**
GTI - EW	0.35	260	East	West
GTI - NS	0.45	100	West	East
BARD - EW	0.1 -> 0 -> 0.2	80 -> 0 -> 270	West -> East	East -> West
BARD - NS	0.2 -> 0 -> 0.3	100 -> 0 -> 290	West -> East	East -> West
GTI - EW horizontal	0.3 -> 0.1	250	East	West
GTI - NS horizontal	0.25 -> 0.4	105	West	East

From the particle drift trajectories, it can be seen that the residual currents during the surveys generally had a north-westerly direction with speeds around 0.02 ms^{-1} and water masses ~ 5 - 8 km to the West - northwest had temporarily been within the OWFs in the last 10 days. Tidal ellipses had a magnitude of ~ 6 - 9 km in an East-West direction (Fig. 2).

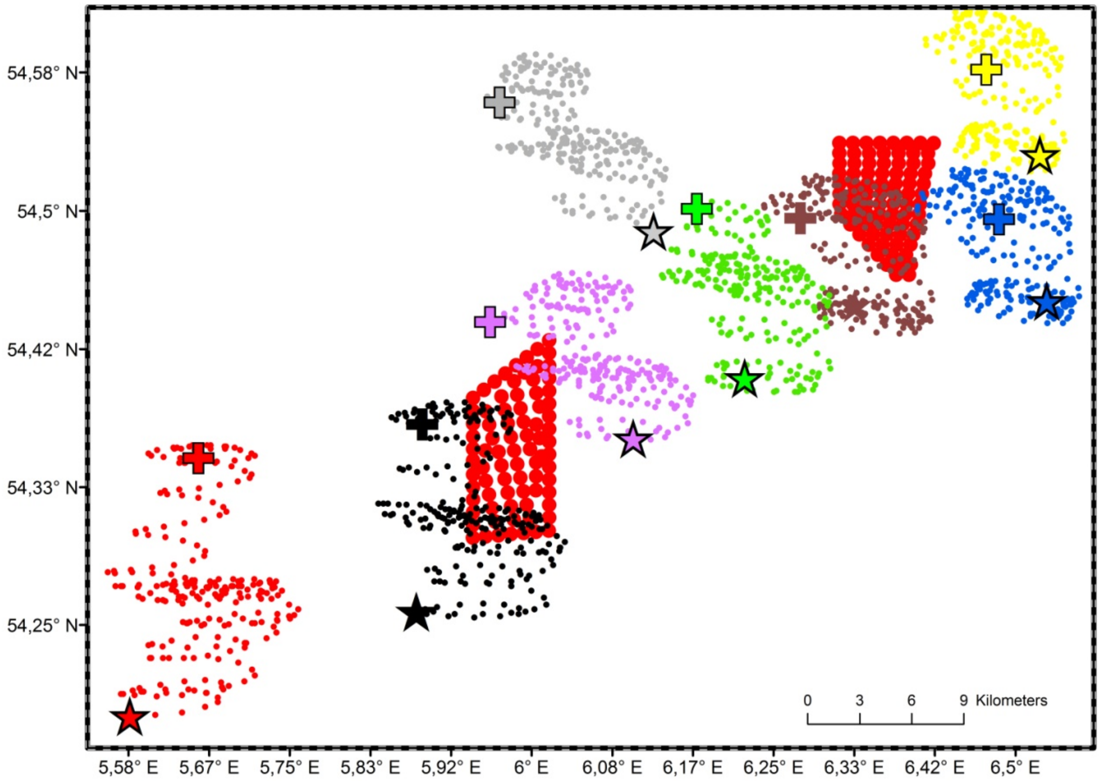

Figure 2: Simulated drift routes (small dots) of eight (colours) exemplary particles for a 10 day period. The starting points are marked with a star symbol and the sampling station by a cross. The former corresponds to the particle position 10 days prior to sampling. The locations of the turbine foundations in the BARD and GTI OWFs are represented by red dots.

Regional SST and chlorophyll-a distribution

MODIS SST data taken during the night of the 23rd July 2014 of the area around the two OWFs show a narrow range between 18.5°C and 19.5°C. Generally, SSTs increased from southeast to northwest, with a patch of colder surface water between the two OWFs (Fig. 3). MODIS derived chlorophyll-*a* data followed the SST distribution: generally decreasing from high values (2.5 mg m^{-3}) in the southeast area to 0.5 mg m^{-3} in the northwest (Fig. 3). The two OWFs were situated within a region of < 1 mg m^{-3} concentrations and temperatures of ~ 19.4 °C. Higher concentrations are found in the patch of colder water (< 19°C) between the two OWFs.

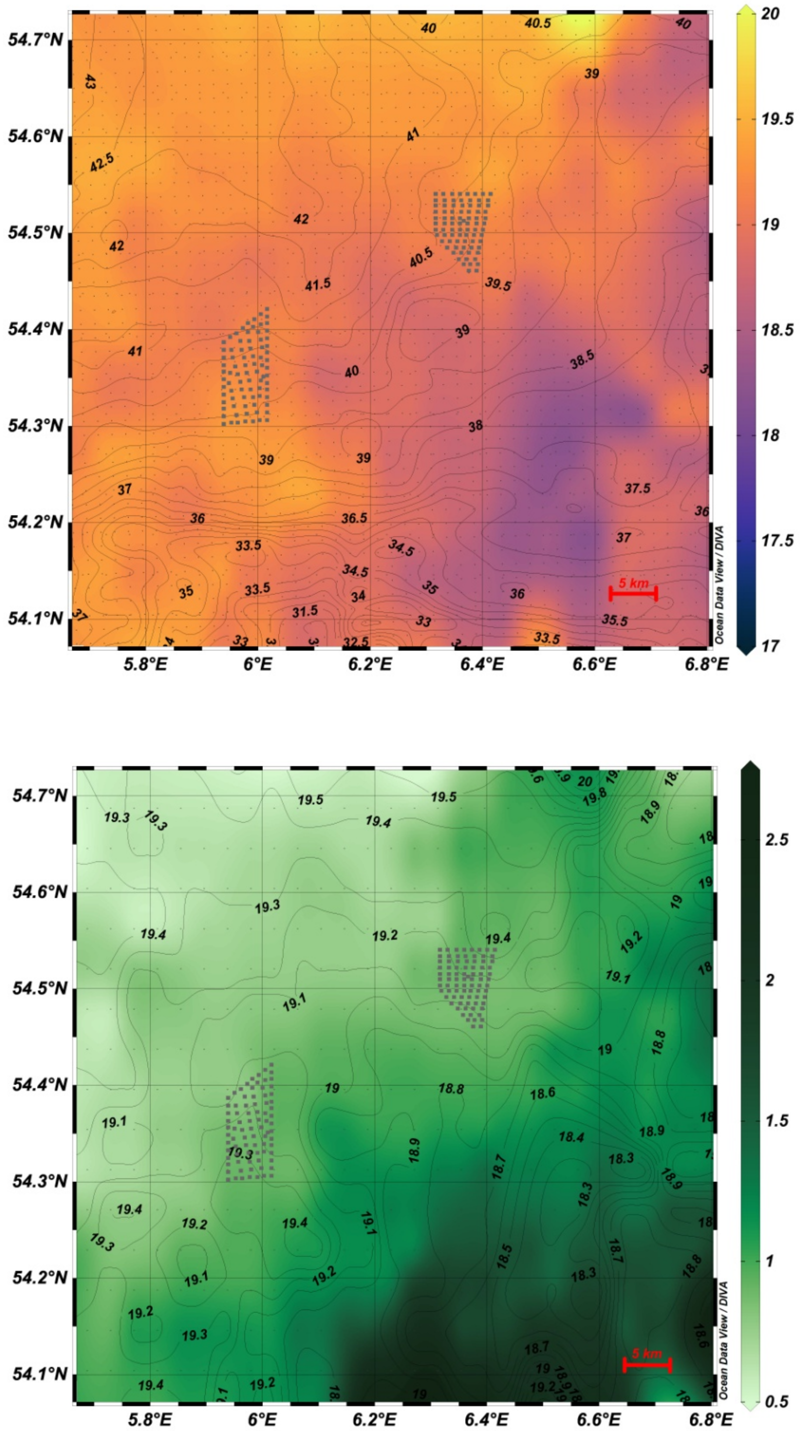

Figure 3: Upper panel: Colour contours of MODIS sea surface temperature (SST, °C) overlain by the location of the OWFs BARD and GTI (grey dots) and bathymetry [m] (black line contours). Lower panel: MODIS chlorophyll-*a* (µg l^{-1}, green colour) overlain by the location of the OWFs BARD and GTI (grey dots) and line contours of the MODIS derived SST [°C].

Local hydrography

All TRIAXUS transects revealed doming of the thermocline within the OWFs, which coincided with a reduced stratification of the water column. This indicates more intense vertical mixing within the OWF than outside, transporting surface water to deeper layers and bottom water upwards. A potential source of this increased mixing is the presence of the 80 wind turbine foundations.

Global Tech I

The 17 km long East - West transect through GTI was sampled on July 19th from 7:27 to 8:30 UTC. The distance between two undulation peaks was ~ 560 m. Salinity was around 34 with small East-West and surface-bottom gradients (Fig. 4). Thermal stratification was evident, with temperature decreasing from 19 °C at the surface to 14 °C at a depth of 30 m. East of the OWF a well-defined thermocline occurred at a depth of 13 m, which spanned between 1m and 8 m. The ~ 6 km long section inside the OWF was characterised by increased variability in the depth of the thermocline and a shallower surface mixed layer (SML). Water density changes followed the temperature profile and the stratification index minima (< 34 Jm^{-3}) were found within the OWF on the downstream side.

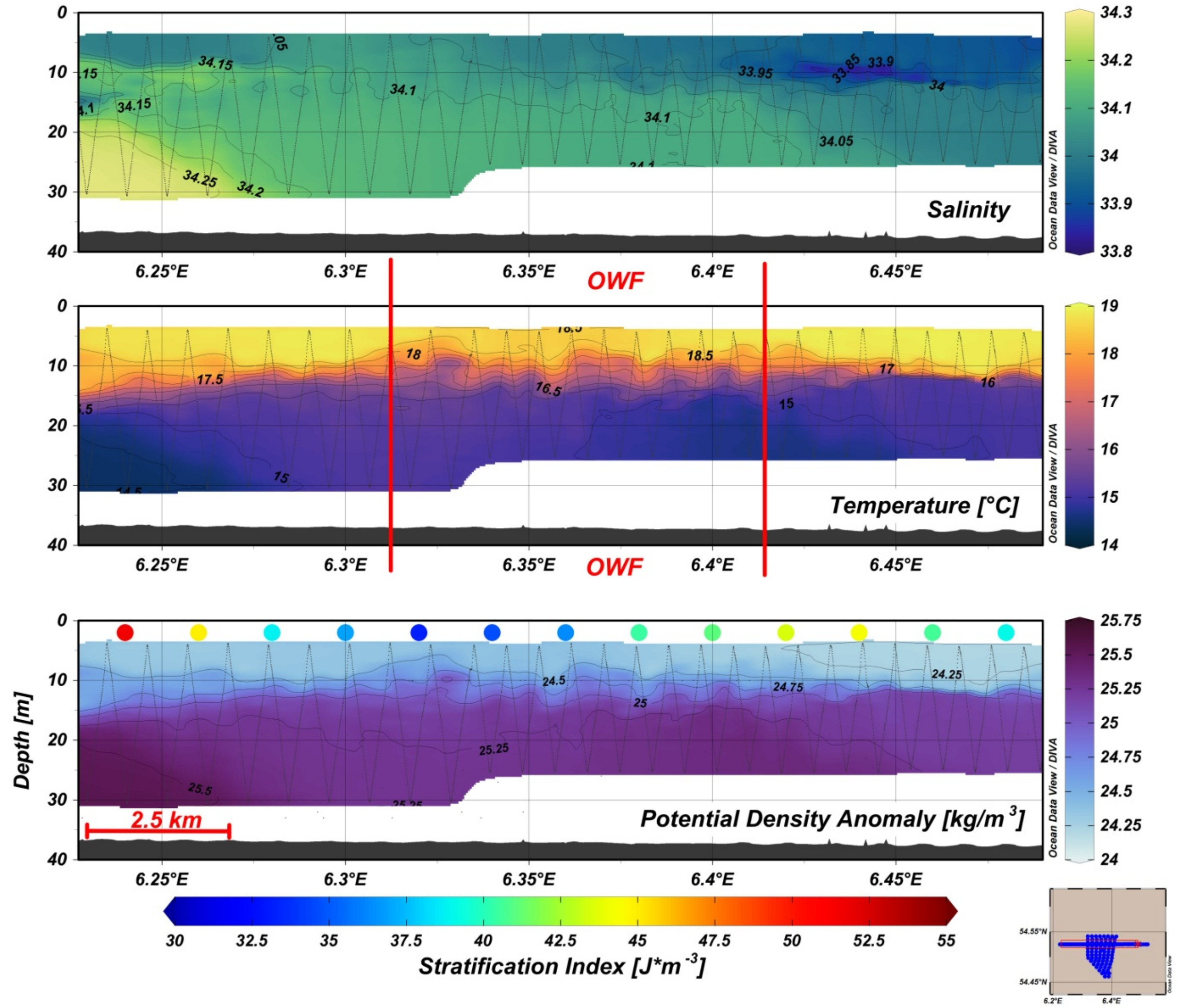

Figure 4: Hydrography of the East - West transect through GTI: colour contours of salinity (upper panel), temperature (mid panel), and potential density anomaly (lower panel). The stratification index is shown as coloured dots in the lower panel (bottom colour bar).The vertical red lines mark the edges of the OWF. The thin black lines depict the TRIAXUS undulation path. The eastern OWF boundary faced the current.

Bard Offshore 1

The 42 km long BARD West-East transect was surveyed from 7:00 UTC to 10:00 UTC on July 23rd, with a 7 km section through the OWF (Fig. 5). Near the beginning of this transect the tide changed, so there was a constant current direction from West to East for ~ 5 hours before reversing to a West-East direction. The western temperature profiles show a deep surface mixed layer that began to rise from 15 m at the western border of the OWF to 6 m 2 km into the wind farm. Underneath the doming thermocline, a cooler 17 °C water mass extended down to 27 m, so that the 16 °C isotherm formed a trough.

In the eastern section of the OWF from approx. 6° E the thermocline de-stabilised and the upper isotherms started to diverge. For another 5 km to 6.2° E the thermocline remained unstable and shallow. Then the surface mixed layer deepened again but the thermocline was not as narrow as west of the OWF. An East-West salinity gradient (34.1 - 34.45) was once again visible, with an intermediate water mass of relatively high salinity water (34.45) lying within the thermocline to the west of the OWF. As this feature is not observed for the computed potential densities and the TS-diagrams are consistent with mixing of water masses between the upper or lower water column and the pycnocline, this feature does not represent an artefact created by thermal lag effects in the conductivity cell. The onset of this intermediate water mass corresponded to the edge of the thermocline doming. The lowest stratification with indices < 27 Jm^{-3} occurred within the OWF and extended approximately 4 km outside of the windfarm, towards the East (Fig. 5).

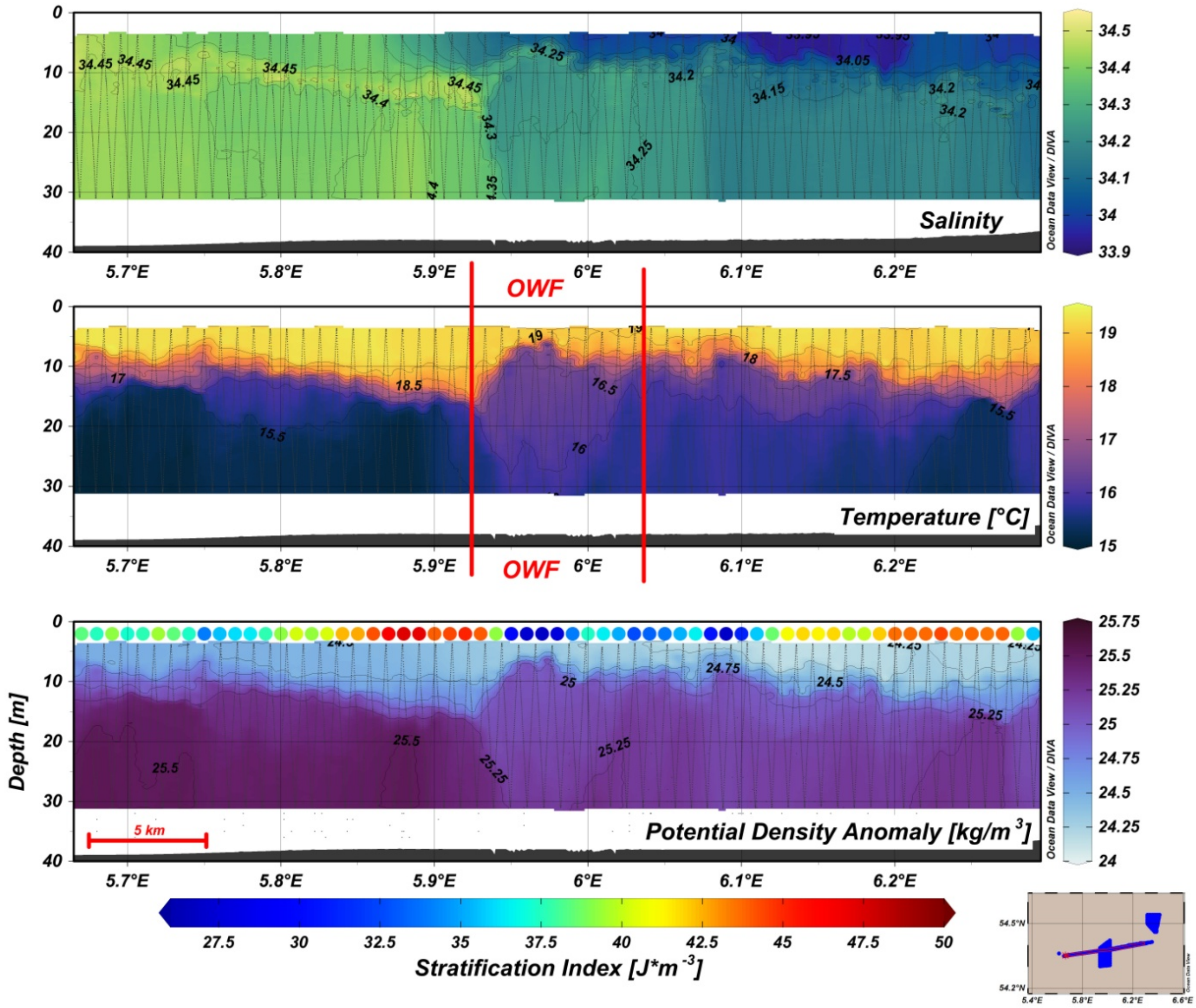

Figure 5: Hydrography of the West-East transect through BARD. See Fig. 4 for a full description.

The 55 km South - North transect started close to the EEZ border (8:00 UTC to 11:45 UTC, July 24th) and included a 14 km section inside BARD. The thermocline showed the same pronounced doming in the centre of the OWF, covering a depth between 4 m to 14 m (Fig. 6). The stratification index had its minimum (< 24 Jm^{-3}) within the wind farm. The narrow thermocline started to widen vertically ~ 18 km north of the OWF. Salinity increased from South to North and the vertical gradient had two features: first, in the OWF the vertical salinity stratification was broken up so that water below the thermocline had a lower salinity than south and north of the OWF; and second, at the northern OWF border a high saline (34.45) water mass with ~ 5 km horizontal extent was situated within and above the thermocline.

At the northern and the southern OWF border we observed horizontal SST minima and the salinity of the water column showed horizontal maxima (Fig. 6). These hydrographic signatures depict zones of local upwelling with surface divergent flows at both latitudinal sides of the OWF.

Before the measurements at the northern OWF border there was a constant West-East current direction for 6 hours whereas the tidal direction was the opposite when we sampled the southern OWF border. Thus, upwelling was visible at the OWF borders which were approx. 90° left to the ambient current direction in both cases.

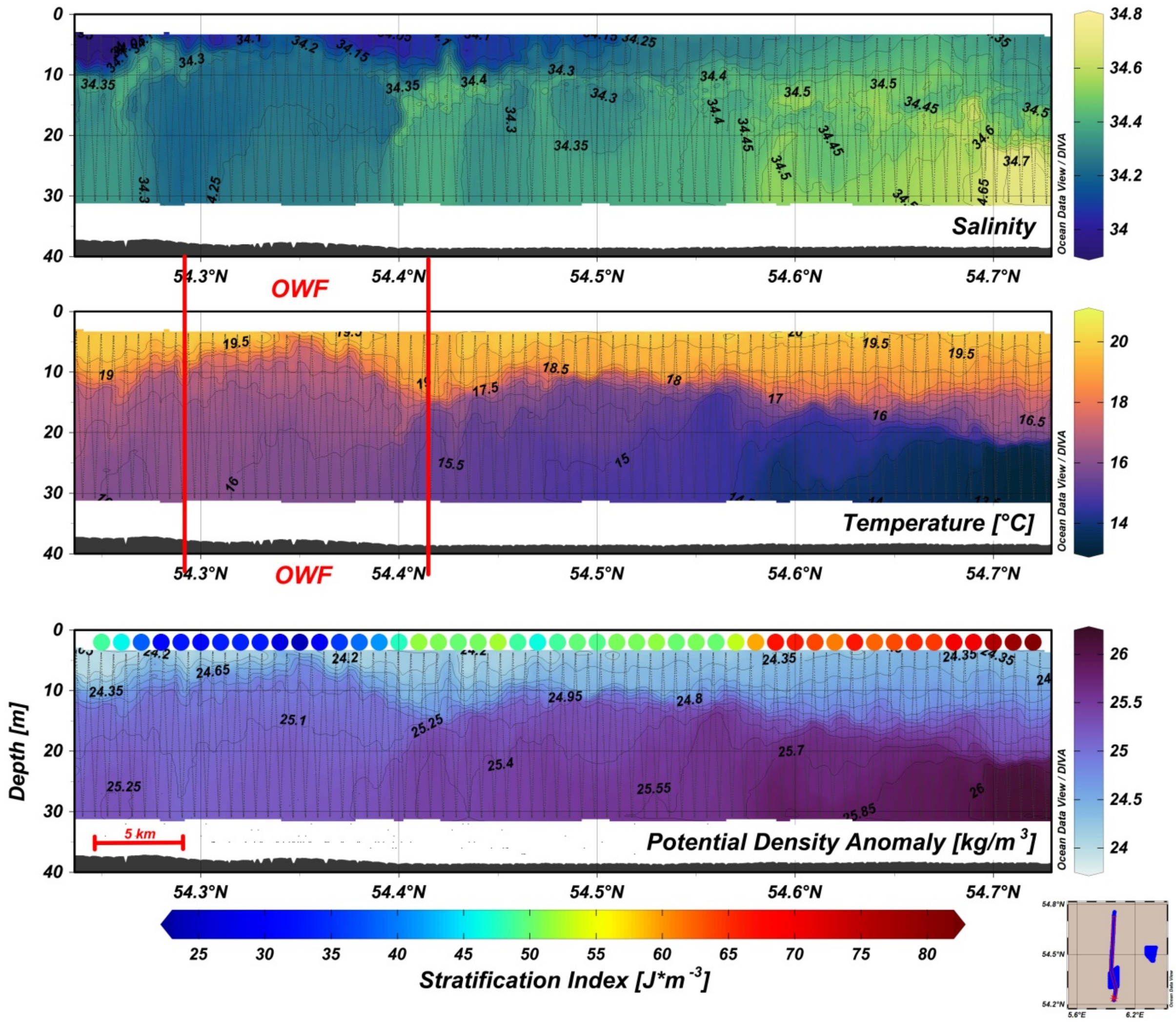

Figure 6: Hydrography of the South - North transect through BARD. See Fig. 4 for a full description.

Phytoplankton & oxygen

The oxygen content along all TRIAXUS transects mirrored the vertical temperature distributions with a tendency for higher values North and East of the wind farms. The phycocyanin fluorescence signal generally had higher values just below the thermocline (see appendix).

Global Tech I

Along the East-West transect through GTI chlorophyll-*a* fluorescence had a distinct maximum at the upstream (eastern) border of the OWF (Fig. 7, second panel), where the thermocline has its largest spread (Fig. 4). In the South-North transect chlorophyll-*a* fluorescence exhibited a row of 3 distinct pillars (1-3 µg l^{-1}) within the wind farm, each with a uniform diameter of approx. 500 m and a uniform spacing of approx. 800 - 900 m (Fig. 7, bottom panel). These chlorophyll-*a* pillars extended vertically from the seafloor into the lower regions of the thermocline. Chlorophyll-*a* patches with variable but broader widths were present outside of the OWF to both the North and the South. The highest chlorophyll-a signals were generally found below the thermocline.

Bard Offshore 1

The chlorophyll-*a* distribution exhibited two pillars west of the wind farm, one column inside and a maximum 5 km east of the wind farm (Fig. 7, top panel). In the region of local upwelling at the northern border of BARD, a patch of high chlorophyll-*a* was located underneath the patch of high saline water. A similar but weaker signal was visible at the southern OWF border. A series of narrow (< 500 m, 1-4 µg l^{-1}) chlorophyll-*a* pillars were observed 3-7 km north and south of the OWF (Fig. 7, third panel).

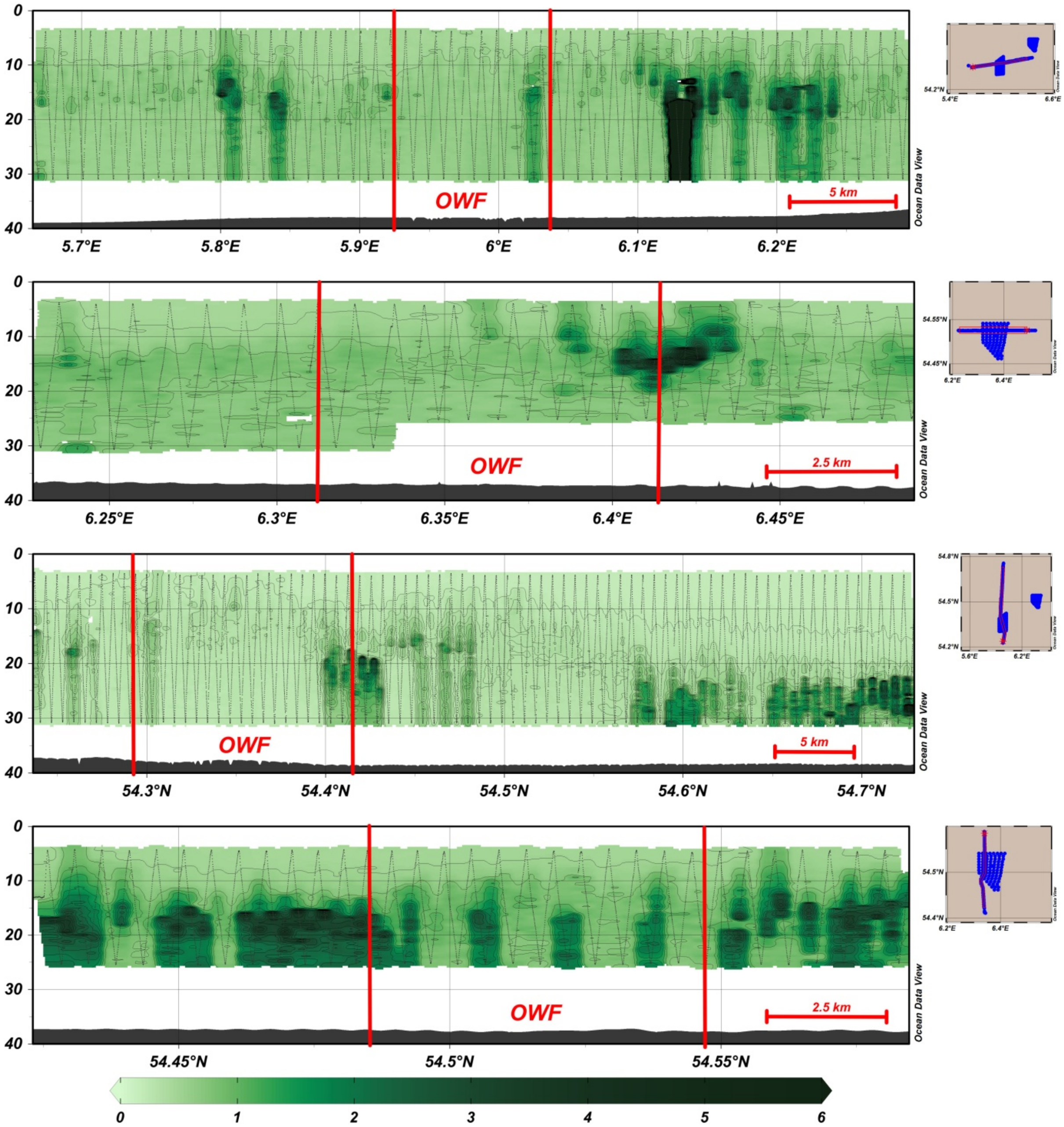

Figure 7: Colour contours of chlorophyll-*a* ($\mu g\ l^{-1}$) transects through the OWFs. From upper panel to lower panel: East - West transect through BARD and GTI, North-South transect through BARD and GTI. The vertical red lines mark the edges of the OWF area. The thin black lines depict the TRIAXUS undulation path

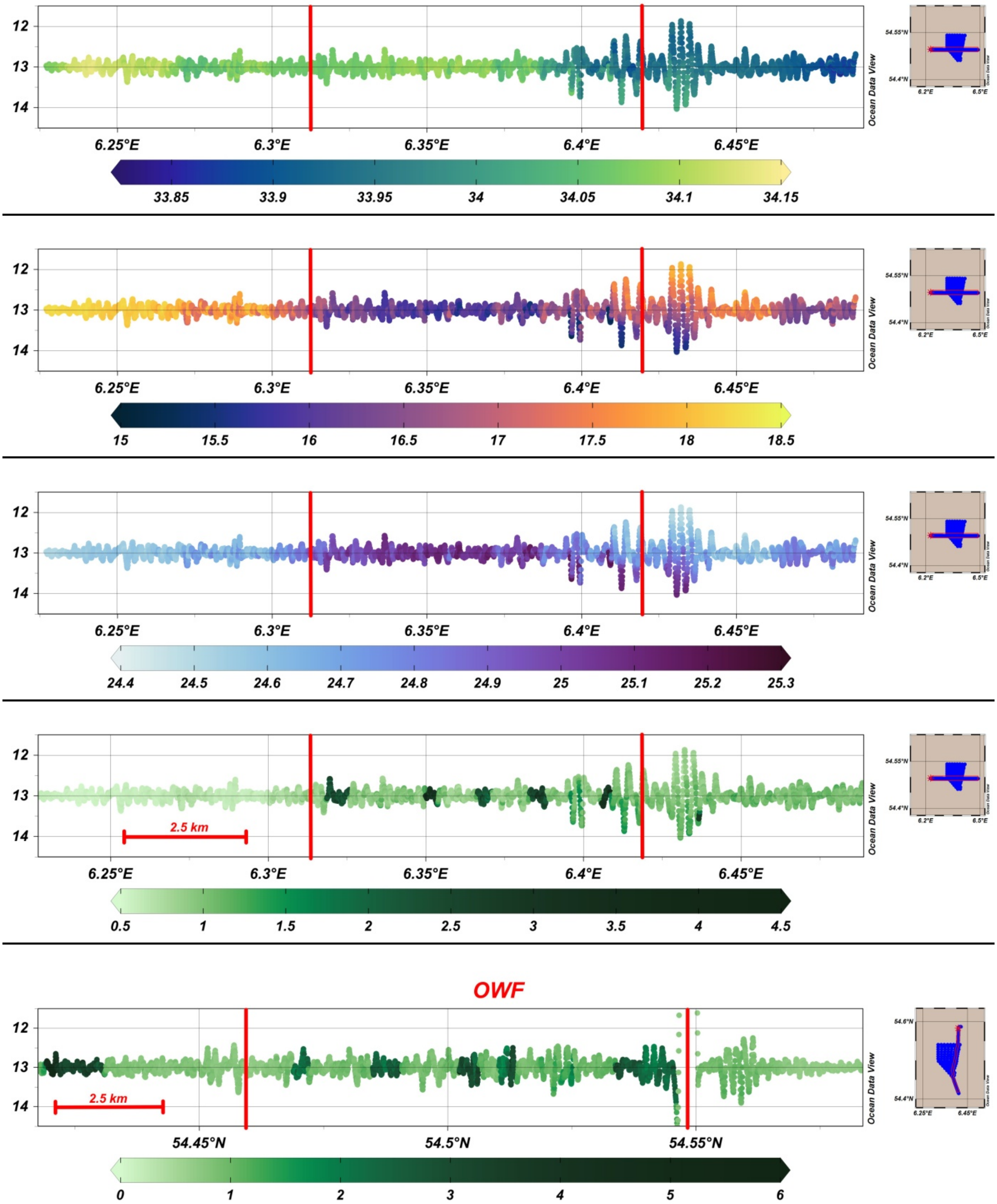

Figure 8: Hydrography of the horizontal transects through GTI: salinity (top panel), temperature (°C, second panel), potential density anomaly (kg m^{-3}, third panel) and chlorophyll-*a* (µg l^{-1}, fourth panel) of the East-West transect and chlorophyll-*a* (µg l^{-1}) of the North-South transect (bottom panel). The vertical red lines mark the section inside the OWF.

Two horizontally stable TRIAXUS tows through GTI at a depth of 13 m showed chlorophyll-*a* patches at the same spatial scales as the chlorophyll-a pillars of the undulating tows (300-500 m width, 700-1200 m distance between patches, Fig. 8). The chlorophyll-a patches found in the horizontal tows were associated with lower temperature values indicating their origin from deeper water layers.

Pre-OWF hydrography in the GTI area

The 22 km long South-North ScanFish transect was sampled on the 14th of July 2010, before the construction of the OWF. The water body was more stratified than in 2014 with temperatures below 10°C at a depth of 30 m and above 18°C close to the sea surface (Fig. 9). From the South to the North the salinity below the thermocline increased from 33.5 to 33.8, while temperature decreased from >11°C to below 10°C. This lead to the highest water column stratification (82.8 Jm^{-3}) at the northern end of the transect. To the South temperature and salinity isolines deepen towards the sea floor, most likely indicating the edge of a tidal front, leading to a stratification minimum (63.8 Jm^{-3}). In the centre of the transect the isotherms spread, producing the smallest surface mixed layer depth (~8 m) and a maximum vertical extent in the thermocline (~18 m). This resulting local stratification minimum (73.3 Jm^{-3}) lies directly within the future location of the OWF GTI. Chlorophyll-*a* was highest within a ~ 3 km long patch at the southern border of the future OWF area, and extended from the seafloor to the lower thermocline (Fig. 9). A second chlorophyll-*a* fluorescence pillar with a length of ~ 1.5 km was located ~ 5.5 km further North. This smaller patch was connected with a broader area of high fluorescence below a depth of 25 m.

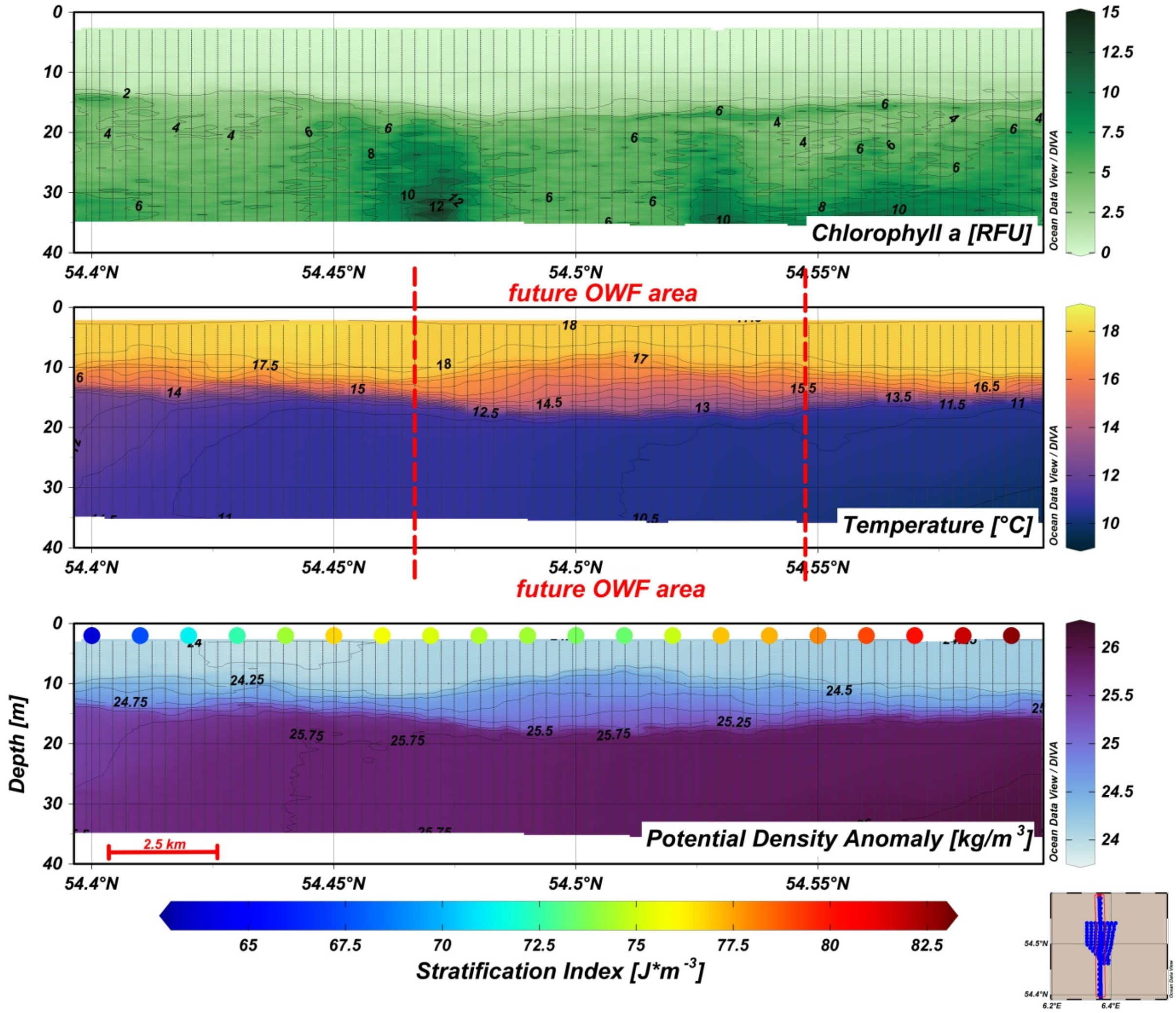

Figure 9: Hydrography and chlorophyll-*a* of the July 2010 pre-OWF SCANFISH South - North transect through the GTI area. Chlorophyll-*a* (relative fluorescence unit (RFU), upper panel), temperature (mid panel), potential density anomaly (lower panel) and stratification index (coloured dots in lower panel,

bottom colour bar). The dashed vertical red lines mark the section inside the future OWF area. The thin lines depict the horizontal gridding resolution.

<u>Nutrients</u>

The nutrient concentrations were generally very low at the surface and increased with depth: nitrate < 0.5 µmol l^{-1}, phosphate < 0.1 µmol l^{-1} and silicate < 3 µmol l^{-1} (see figures in the appendix).
Nutrient concentrations were plotted by depth stratum (surface, thermocline, bottom) versus the PELETS particle drift model derived OWF contact times, i.e., duration, which the analysed water body previously spent in an OWF. When all stations were analysed together no relationship was visible. However, for the GTI East-West transect, the only one with a high fraction of non-zero contact times, surface layer chlorophyll-*a* (r^2 = 0.48), silicate (r^2 = 0.46) and phosphate (r^2 = 0.27) concentrations showed a linear increase with contact time. Nitrate concentrations followed an optimum function with a peak for a ~ 50 hours (h) OWF contact time (r^2 = 0.51). Ammonia (r^2 = 0.35) and nitrite (r^2 = 0.32) showed linearly decreasing concentrations with increased contact times (Tab. 2 and figures in the appendix).

Table 2: Relationships between surface layer (5m depth) nutrient concentrations [µmol l^{-1}] and the time the analysed water mass spent in an OWF [h]. Chl-*a*: mean chlorophyll-*a* [µgl^{-1}] of surface and thermocline water samples. No relationship: #, significance levels: * p < 0.1, ** p < 0.05

	all stations combined	GTI EW	GTI NS	BARD EW	BARD NS
Stations [N]	62	11	11	22	11
Stations with OWF contact [N]	25 (40%)	10 (91%)	2 (18%)	8 (36%)	5 (45%)
Max duration [h]	118	99	2	118	36
Chl a	#	Linear increase *	#	#	Linear increase *
Silicate	#	Linear increase **	#	#	Linear increase
Ammonia NH4	#	Linear decrease *	#	#	#
Nitrate NO3	#	Optimum **	#	#	Linear decrease *
Nitrite NO2	#	Linear decrease *	#	#	#
Phosphate PO4	#	Linear increase	#	#	Linear increase
Dissolved inorganic nitrogen DIN	#	Linear decrease *	#	#	#

<u>Light</u>

A flattening of the 1% PAR depth was observed, which decreased from 25.7 m at the OWF borders to a minimum of 20 m inside the OWF. The daylight (GR 600-800 W m^{-2}) vertical PAR profiles revealed values above 10 µmol m^{-2} s^{-1} at 25 m depth enabling net primary production well below the thermocline (Fig. 10). Calculating primary production with 10 µmol m^{-2} s^{-1} with the PE-curves obtained during the cruise, resulted in 8-20% of maximum primary production. However, the flattening of the 1% PAR depth was not observed during the other three undulation transects through the OWFs (see appendix).

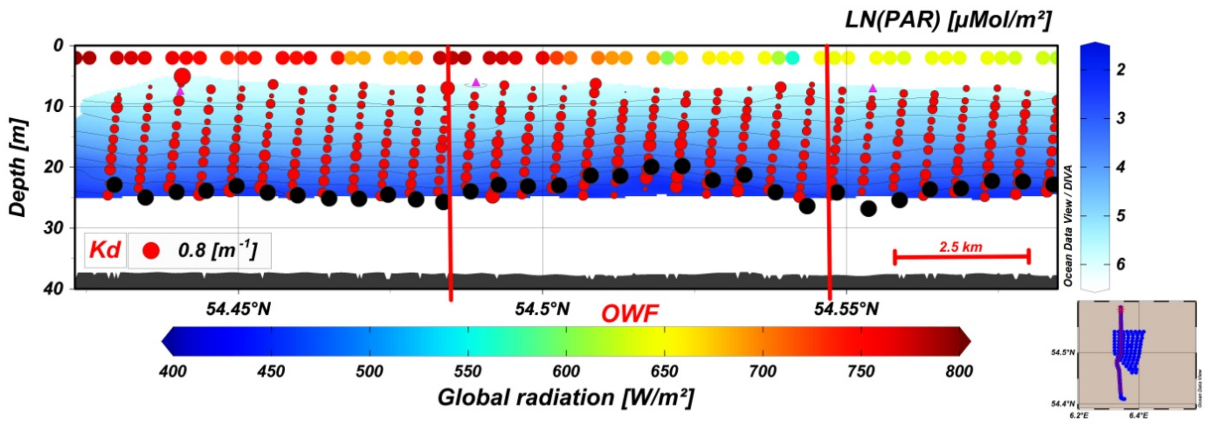

Figure 10: North - South transect through GTI. Log scale PAR (blue shading) and global radiation (filled circles corresponding to the bottom colour bar). The red dots are scaled to the diffuse attenuation coefficient Kd, where triangles depict omitted negative values. The black dots represent the 1% PAR depth. The vertical red lines mark the edge of the OWF area.

<u>Zooplankton</u>

The fine resolution data obtained from the VPR revealed group specific zooplankton densities that showed distinct distribution patterns in relation to the OWFs and ambient hydrography.

Global Tech I

Copepoda were evenly distributed in the horizontal, with concentrations of up to 9 organisms l^{-1} within the thermocline and SML. Pilidium larvae of nemertean worms were confined to the thermocline along both transects. Gastropoda veliger larvae were mainly found in the SML (Fig. 11), while cladocerans occurred only north of GTI in low concentrations and more easterly in lower saline water. Pluteus larvae, i.e., pelagic larvae of benthic sea urchins or brittle stars, were found in the areas west of GTI, i.e., at the residual downstream side. Dinoflagellates and small jellyfish (e.g. Pleurobrachia spp.) were spread evenly across the transects and the water column, while copepod nauplii were mainly observed in the deeper layers (see Appendix).

Bard Offshore 1

High concentrations (up to 35 N l^{-1}) of meroplanktonic pluteus larvae, mainly from brittle stars and to a much lesser extent from sea urchins (ICES, 1964), were observed at the intermediate high saline (34.45) water mass around the thermocline to the west of the OWF (Fig. 12) and at the local upwelling zone to the north of the OWF. The LOPC detected these pluteus larvae with a size range of 0.45-1.92 mm equivalent spherical diameter (ESD, see appendix). Late ophiuroidea (brittle star) larvae in their settlement phase were found in the deep waters within and west of BARD Offshore 1. According to the particle drift model results (Fig. 2), the water mass with high meroplankton densities West and North of BARD Offshore 1 passed through the wind farm area. Samples between the two OWFs as well as further North and East probably originated from water bodies without contact to the wind farm areas. Marine Snow had maximum concentrations below the thermocline, especially in areas with low copepod densities, so that extreme values of both never co-occurred (Fig. 12 and appendix). Furthermore, enhanced concentrations occurred in the SML within and east of the OWF. Polychaeta (Pectinariidae) larvae occurred mainly in the western and southern areas.

Dinoflagellates occurred in the SML and thermocline in higher salinity water to the North and west of the OWF. Finally, copepoda, marine snow and pilidium larvae showed similar distributions to the GTI transects.

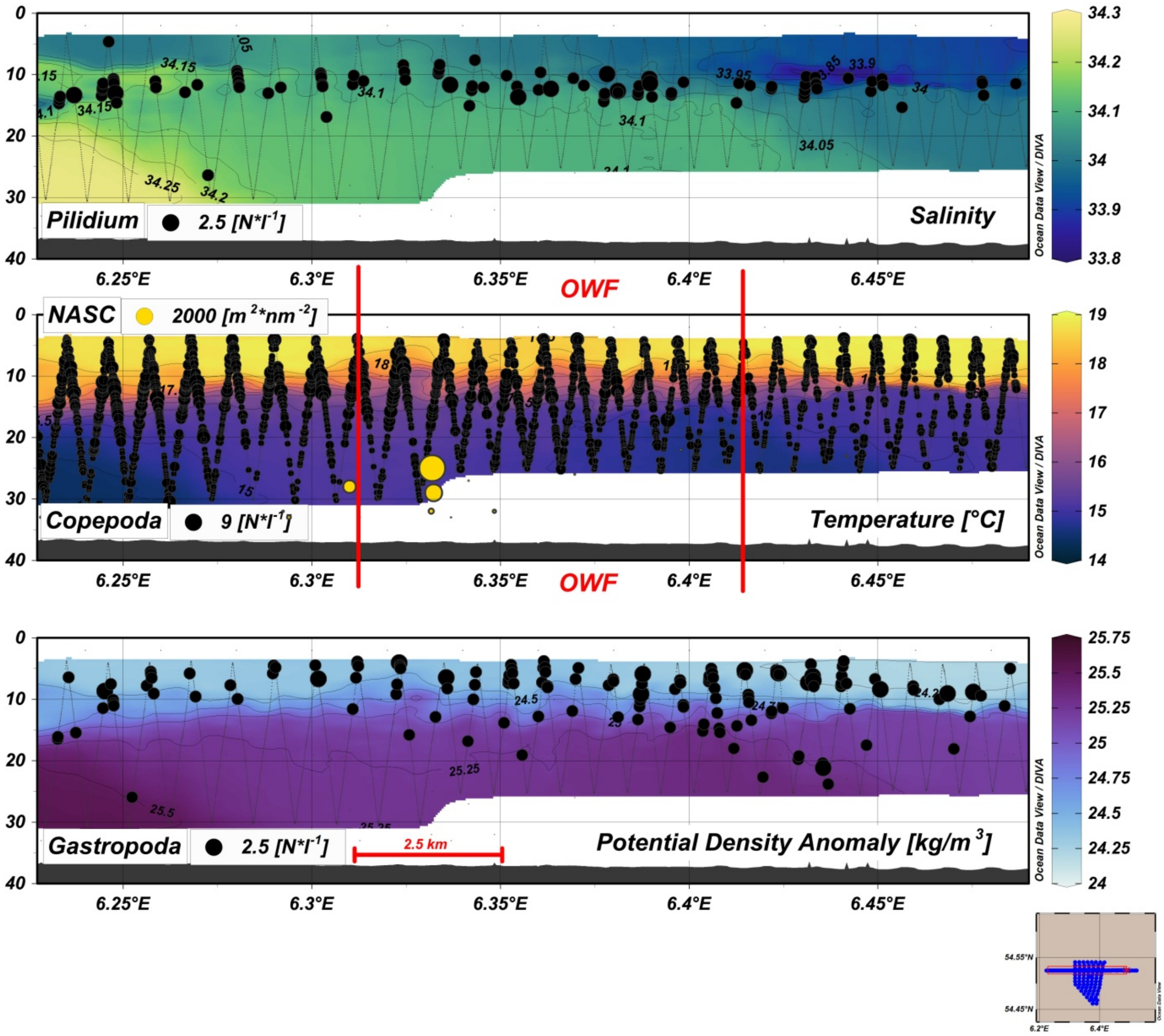

Figure 11: Plankton (black dots), fish distribution and hydrography of the East - West transect through GTI: pilidium larvae and salinity (upper panel), copepods and temperature (mid panel), gastropoda veliger larvae and potential density anomaly (lower panel). Pelagic fish schools as Natuical Area Scattering Coefficients (NASC, yellow dots in mid panel). The vertical red lines mark the section inside the OWF.

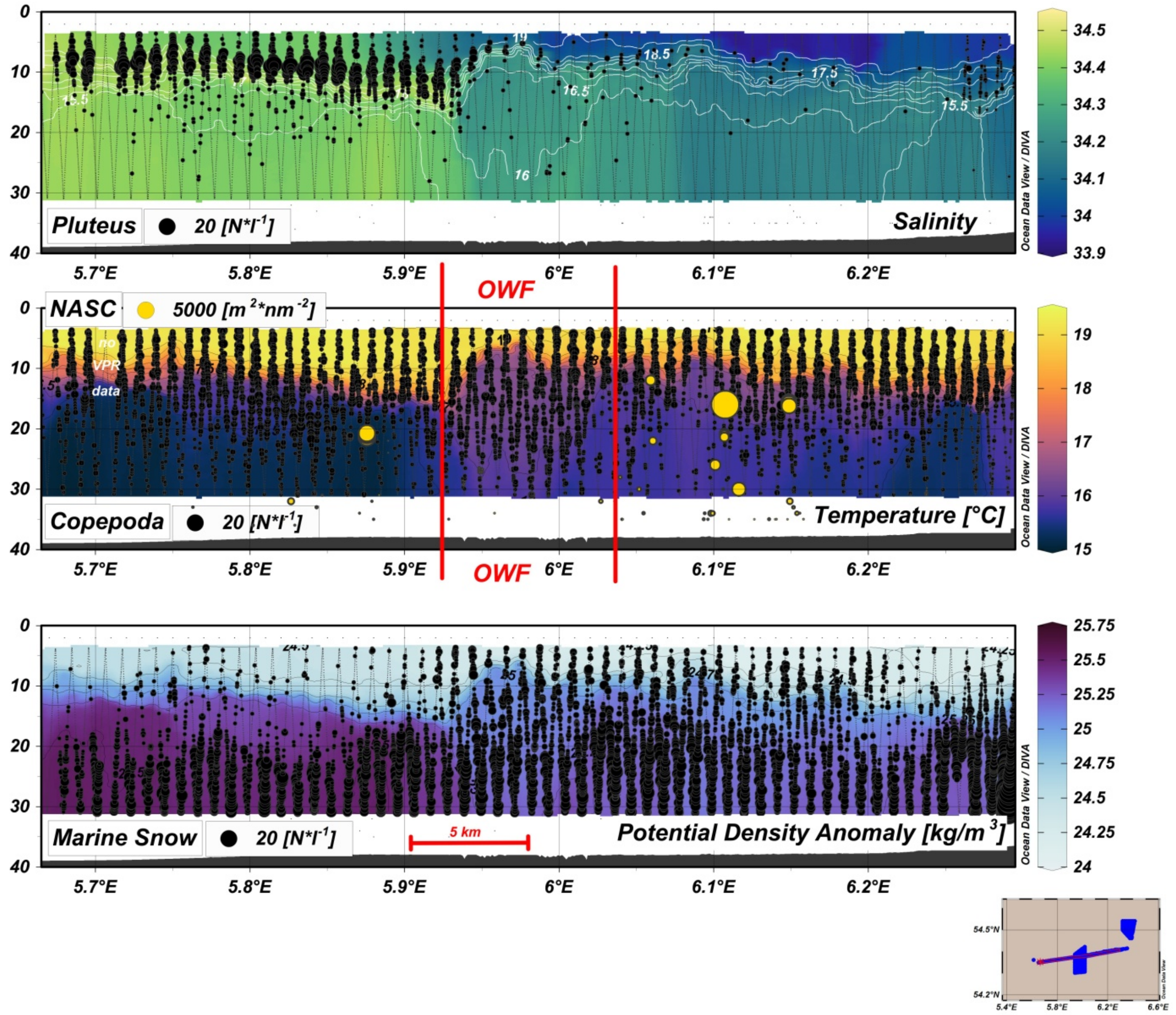

Figure 12: Plankton (black dots), fish distribution and hydrography of the West - East transect through BARD: pluteus larvae and salinity (upper panel), copepoda and temperature (mid panel), marine snow and potential density anomaly (lower panel). Pelagic fish schools as Natuical Area Scattering Coefficients (NASC, yellow dots in mid panel). The vertical red lines mark the section inside the OWF.

The net-samples showed that copepods were the most abundant taxonomic group and provided more than 80% of the plankton organisms in 95% of all WP2 samples. Of the 19 net samples, 2 were located inside an OWF and one was taken from a water mass that had previously passed through an OWF. The zooplankton compositions derived from the WP2-net samples did not show any relationship with nutrient concentrations or with the time the water bodies spent in an OWF.

<u>Fish distribution</u>

The analysis of the 38 KHz hydroacoustic records showed the typical patchy spatial distribution of pelagic fish schools (Figs. 11-13). Their visual occurrence and frequency response (Fernandes et al., 2006) qualified them most likely as clupeids, i.e., the regionally dominant planctivorous species herring (*Clupea harengus*) and sprat (*Sprattus sprattus*). As clear spatial trends were not visible, we divided the results into five regions for each of the two OWFs: one within the OWFs and the others as the four quadrants around them. As the tidal ellipses were spanning an East-West distance of ~ 7 km, we defined North-West, North-East, South-West and South-East quadrants with a maximum distance of 3 nmi (5.6 km) from the GTI area (BARD, 4 nmi, 7.4 km, Fig. 13). Looking at this spatial scale, median pelagic fish densities were higher within the OWFs and in the northwestern quadrants. However, variability was high and high densities occurred in other quadrants as well. Thus, no statistically significant differences existed between the five regions (white circles in Fig. 13): mean NASC [m^2/nmi^2]: 248 (BARD), 91 (GTI), 160 (outside OWFs); cv`s: 187% (BARD), 123% (GTI), 270% (outside OWFs).

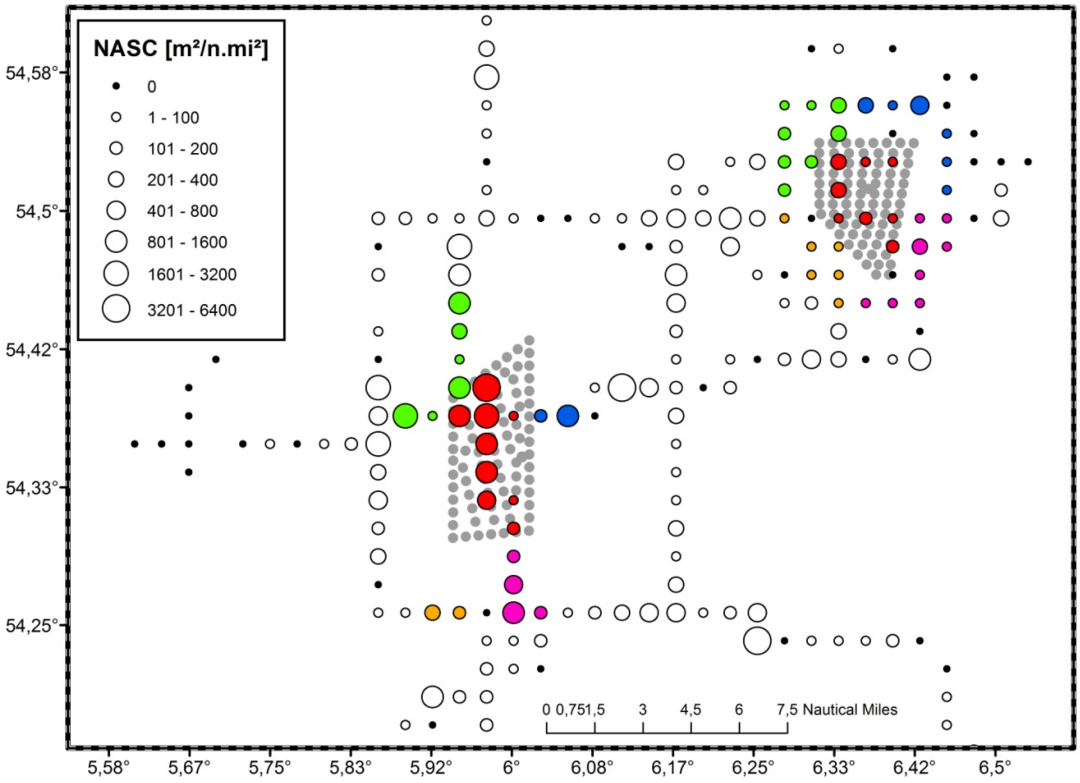

Figure 13: Distribution of pelagic fish schools as mean nautical area scattering coefficients (NASC [m^2/nmi^2]) at a 1 nmi grid. Colours depict the regions: red: inside OWF, northwest: green, northeast: blue, southeast: pink, soutwest: orange, outside: white. Wind turbines: grey dots.

Discussion

<u>Ambient hydrography</u>

The two surveyed OWFs, BARD Offshore 1 and Global Tech I, are located approx. 100 km offshore in the German EEZ with water depths of around 40 m, and cover areas of 59 km^2 and 41 km^2, respectively. The ambient water body has been categorized as Southern North Sea Water (NSTF, 1993) with a typical salinity range of 34 - 34.75. The location is in the southern part of region A5, a region characterised by an East-West salinity increase (Lee, 1980, Huthnance, 1991) and north of the Regions Of Freshwater Influence (ROFI, van Leeuwen et al., 2015). According to Lee (1980) and Huthnance (1991) the survey areas is north of region A4 Continental Coastal Water, so east and south of GTI an influence of less saline (31 - 34) water is to be expected.

A recent long-term analysis described the survey area as a transitional region with large interannual variability in stratification and subsequently in the occurrence of tidal fronts (van Leeuwen et al., 2015). The two OWFs are in an area which was categorized as occasionally stratified (Becker et al., 1992) as they are located in the transition zone between mixed and stratified water (Krause et al., 1986). Seasonal thermal stratification generally occurs north of the 40 m depth contour, or north of about 54°N (Huthnance, 1991). Therefore, the typical early summer stratification is expected to break down in August (Lee, 1980, Huthnance, 1991), after our surveys were completed.

Water currents

During the survey period the vertically integrated residual currents were flowing predominantly from the southeast to the northwest (Fig. 2 and appendix). This is in contrast to the predominantly occurring summer residual current that flows from the Southwest to the Northeast (Lee, 1980, see appendix). The tidal ellipses were spanning an East-West distance of ~ 7 km, matching the dimensions of the OWFs. Typically, the daily averaged residual currents from the TRIM model can be reconstructed from its first three principal components (PC) (Callies et al., 2016). However, this did not work for the beginning of the survey period (19th -20th July 2014), suggesting a locally more complex current regime (see appendix). The first PC describes a shift from a cyclonic residual current regime before July 19th and an anti-cyclonic pattern from July 22 onwards. The cause might have been the high southeasterly wind speeds (>14 ms^{-1}) that prevailed during the night on July 19th before it calmed down on the 20th - 21st July and shifted to northeasterly directions at 5-7 ms^{-1} (see appendix).

Effects of the OWF

The key objective of the survey was to provide empirical evidence of potential effects of OWF turbine foundations on ambient hydrography, local nutrient concentrations, plankton densities and fish distribution.

Stratification

As the tidal currents flow past the OWF foundation structures they will generate a turbulent wake that is expected to contribute to a mixing of the stratification (Cazenave et al. 2016, Carpenter et al. 2016). In order to assess this effect of the OWFs on the stratification the stratification index is plotted for each transect in Fig. 14. It can be seen that in each case the minimum of the stratification index is observed within the OWF, which shows a drop from that generally seen outside the OWF. However, caution must be used when associating this drop in the stratification index with OWF-induced mixing. The black curve in Fig. 14 also shows a drop in the OWF, despite having been measured in 2010, before the construction of the GTI farm. The identical geographic location of the local stratification minimum in the area of the future OWF points towards the possibility that natural factors favor their occurrence at this position. This could result from the interplay between tidal currents and bottom topography, known to define typical frontal regions (Bowers & Simpson 1987, Schrum, 1997, Holt and Umlauf, 2008).

Also apparent in the stratification index curves is a natural background variability. Comparing the results with the pre-OWF ScanFish transect and other studies (Hill et al., 1993, North et al., 2016), it can be deduced that, in summer for this region, a 20%-50% stratification reduction over a distance of 2-3 km may fit into the corridor of natural spatio-temporal variability. As North et al. (2016) pointed out, horizontal and/or vertical advection within a submesoscale eddy or front can produce isotherm doming and subsequent decreases in stratification. In order to attempt to remove some of the large-scale background variability of these curves, we also detrended the data based on a linear fit in Fig. 14 (lower panel). This shows that the drop in the stratification index coincident with the wind farms is greatest in the transects with already built OWF structures.

It should be noted that since the tidal excursion distance in this region of the North Sea close to both OWFs is approximately the same distance as the farms themselves (see Fig. 2). We expect that this will also cause advection of the stratification index minimum within the OWF depending on the tidal phase, as can also be seen in Fig. 14.

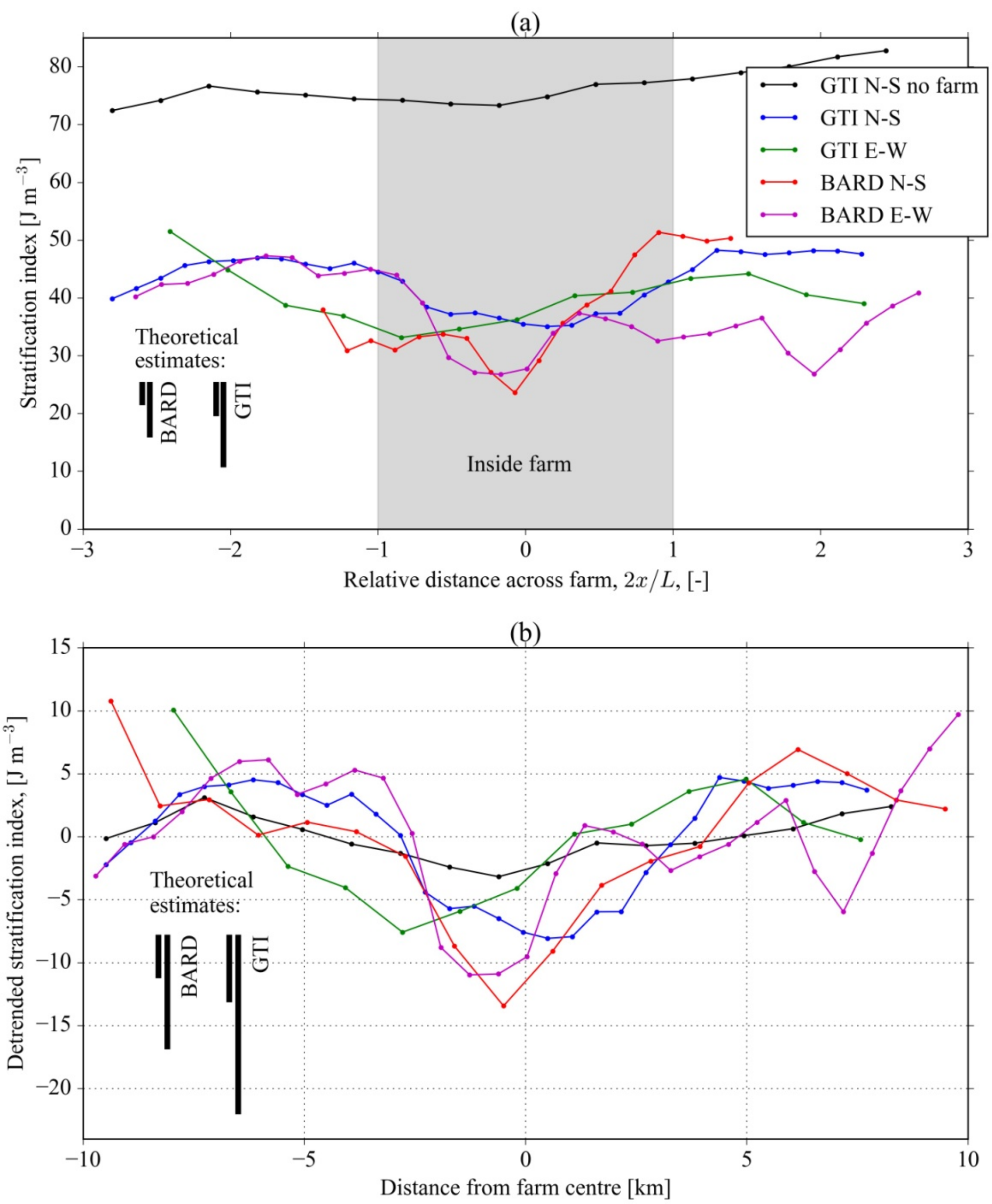

Figure 14: Stratification indices for transects through BARD and GTI. Both the wind farm and the direction of the transect (i.e., North-South or East-West) is indicated by the different coloured curves in the legend. In the upper panel the horizontal distance has been normalized by the width of the farm (L) so that the farm position lies between -1 and 1 for each transect (grey shading). Theoretical estimates of the drop in stratification index for each farm, and each turbulence scenario, are indicated by the length of the black bars in both panels. The lower panel shows the stratification index from above after

a linear detrending, and with a horizontal distance axis centred with respect to the farm and in units of kilometres.

It is also possible to compare the observed drops in the stratification index with the idealized model of Carpenter et al. (2016). In this study an order-of-magnitude estimate of the mixing induced by the OWF structures can be found given the following: (i) the time a water column is expected to spend in the enhanced mixing region of an OWF, (ii) estimates of the mean thermocline thickness, and (iii) estimates for the power delivered to turbulent mixing by the OWF structures. Based on the simulated drift routes from Fig. 2, we can estimate an approximate duration of 10 days for the enhanced mixing of a water column. This can then be combined with an approximate thermocline thickness of 10 m (see Fig. 4,5,6), and the turbulence estimates for the BARD and GTI farms provided in Carpenter et al. (2016), to produce the estimated drops in stratification index that are shown in Fig. 14. Two different high- and low-turbulence scenarios are presented in Carpenter et al. (2016) based on uncertainties in the drag coefficient of the foundation structures. These are shown as the two different bars for each OWF. In addition, the geometry of the foundations and their horizontal density contribute to differences between BARD and GTI. In general, given the many simplifying assumptions of the theoretical estimates, there is decent agreement between the observed drop in stratification index, and that predicted from the theoretical model. These results suggest that OWF foundations are responsible for at least part of the observed increase in vertical mixing, which are also being enhanced by local tide-bathymetry interactions.

Increased mixing / local upwelling

According to previous modelling analyses (Lass et al., 2008, Rennau et al., 2012, Cazenave et al., 2016), corroborated by remotely sensed images (Li et al., 2014; Vanhellemont and Ruddick, 2014), one can expect wakes with a length of ~ 1 km for each of the 80 turbine foundations present in the OWFs. As the wind turbine foundations are 900-1000 m apart, the wakes may have the potential to enhance vertical mixing inside the entire OWF, as indicated in the salinity and temperature profiles of our four transects through GTI and BARD.

The observed zone of local upwelling with surface divergent flows at the latitudinal borders of BARD may be a cumulative result of all turbine foundations in the OWF: an increase in vertical mixing and a decrease in current speed within an OWF may lead to the formation of small-scale features like fronts and eddies (Cazenave et al., 2016).

Simpson et al. (1982) surveyed an island in a stratified region of the Celtic shelf sea and observed a local increase in tidal mixing, subsequently fronts and high chlorophyll-a concentrations in the pycnocline occurred. So, as an island has a stirring effect (Simpson et al.,1982) an OWF in a tidally affected stratified sea may also create a stirring effect, with tidally pulsed local upwelling cells along the sides that are parallel to the currents.

Further indication of this stirring effect is the increased variability in the vertical movement of the towed TRIAXUS at one border of the OWFs. This was observed when the TRIAXUS was towed at a stable depth of 13 m through GTI (Fig. 8).

Nutrients
The July 2014 SML nutrient concentrations were typically low (Topcu et al., 2011), and only silicate and phosphate concentrations in the GTI EW transect correlated with the duration (range: 0 - 99 hours) of the water body inside the OWF area. In the nutrient depleted summer situation nitrogen may have been the limiting nutrient (Buson et al., 2016). The increase of silicate and phosphate concentrations with the contact time may be explained from local upwelling or increased vertical mixing and from the nutrient ratios below the thermocline: DIN/phosphate ratios below the thermocline were close to the Redfield ratio (mean =17.8, st.dev. = 2.2), silicate/DIN levels were relatively high (mean = 1.9, st.dev. = 0.3) but ammonium/phosphate ratios were lower (mean = 14.3, st.dev. = 2.6). Given that ammonium is the preferred nitrogen species (e.g. Dortch, 1990), and assuming an N/P uptake ratio of ~15 and an N/Si uptake ratio of about 1 (Brzezinski, 1985) upwelling / vertical mixing of nutrients from below the thermocline would lead to a slight increase of phosphate, silicate and initially also of nitrate concentrations. The optimum curve of nitrate levels (see appendix) may indicate that after ~ 48 h with decreasing ammonium levels phytoplankton had switched to nitrate. The switch to nitrate may have been stimulated by a depletion due to increasing phytoplankton biomass.

Primary production and chlorophyll-a
Van der Molen et al. (2014) assessed potential impacts of large-scale operational wind turbine arrays placed in a well-mixed area in the North Sea with weak currents. They applied a coupled physical–biogeochemical model GETM–ERSEM– BFM with a spatial resolution of approximately 11 km. Therefore, they did not consider far field wind wake nor turbine foundation effects on the pelagic system. The authors argued for an increased primary production due to lower suspended matter concentrations and hence higher light availability when the OWF turbines are operating. However, our results suggest otherwise. Van der Molen et al. (2014) also suggested that primary production may be decreased by higher turbulence levels induced by turbine foundations, as seen in satellite images of turbid wakes in OWFs (Vanhellemont and Ruddick, 2014). However, three of four transects showed no differences in light availability within and outside the OWFs, while only the fourth transect showed a 20% reduction in 1% PAR depth (Fig. 10). Further, LANDSAT images (https://landsatlook.usgs.gov) of our survey region taken on July 24th 2014 did not reveal any turbid wakes within BARD or GTI. This may be because the region is much deeper and most likely more stratified than in the area analysed by Vanhellemont and Ruddick (2014). From that we can conclude that changes in light availability due to the OWFs had a minor effect on the primary production during our survey.

The general distribution of chlorophyll-*a* showed a typical summer situation with higher values within the lower margins of the thermocline and the deep mixed layer. The most prominent feature of our chlorophyll-*a* measurements was the frequent occurrence of submesocale pillars, with diameters of ~ 500 m, which often had regular gaps of ~ 800 - 900 m between them (Fig. 7). The chlorophyll-*a* patches and scales were also visible in the two stable horizontal TRIAXUS tows through GTI. The observed pillars were considerably smaller than the 4 km chlorophyll-*a* pillar observed in the German Bight by North et al. (2016). The process creating these small pillars remains unclear as no other recorded parameter corresponds to that pattern. It is also not certain whether the creation of these pillars was related to the OWFs or a naturally occurring process.

One working hypothesis is that they are left-over signatures of dissipated submesoscale features (e.g., eddies) created by the turbine foundations. The inter-patch distance roughly corresponds to the inter-turbine distance of 900 m. The features may have mixed nutrients and phytoplankton cells up to higher light intensities, fueling phytoplankton growth.
As at least some light for net primary production was available below the thermocline (Fig. 10) and Fv/Fm ratios from FRRF fluorometry measurements indicated a good physiological status it can be expected that upwelled phytoplankton cells were viable and immediately increased their production. At some point the submesoscale features dissipated, leaving only the biological signal. Eddies and fronts with spatial scales of hundred meters and temporal scales of hours are a key element of ocean dynamics that is still poorly understood (pers.com. B. Baschek, http://www.uhrwerk-ozean.de/index.html.en). These pillars could also be curtain-like structures resulting from dissipated short-lived submesoscale fronts crossed at a right angle by our transects. Alternatively, these curtains could have also been created in the upwelling areas just outside the OWF and then advected into the wind farm and cut into pillars as they were affected by the von Kármán vortex streets forming behind the turbine foundations. Unfortunately, due to an instrument failure we do not have high resolution ADCP current data that might help to confirm this.
The significance and fate of OWF-increased primary production remains an open task to investigate. Enhanced phytoplankton biomass could have been used by secondary consumers fueling higher trophic levels, which may also create an attractive habitat for pelagic fish when copepod abundance is low. The long-term interplay of advection and residence time of the water body within the wind farm may also determine whether local or distant benthic communities are benefitting. If the increased production of organic material simply sinks to the bottom, it may enhance oxygen depletion in the bottom waters (Topcu & Brockmann, 2015, Große et *al*., 2016, Queste et al., 2016).

Zooplankton
The most interesting features of the zooplankton distribution were the high meroplankton densities in water bodies that previously drifted through the wind farm area. The high concentrations of pluteus larvae point towards the potential importance of the OWFs for echinoderms (Krone et al., 2013). In fact, qualitative analyses of underwater video sequences provided by GTI, from varying but unknown depths, support this hypothesis, as high numbers of sea urchins (Echinus spp.) were visible. Moreover, many common starfish (*Asterias rubens*), sea anemones (Actiniaria), sponges (Porifera) and blue mussels (*Mytilus edulis*) inhabited the foundations. A total of 15 underwater images of foundations in BARD showed a similar community at a depth of 10 m, but sea urchins were less abundant. The wind turbine foundations are obviously a well-accepted artificial benthic substrate habitat.
An exact quantification and differentiation of brittle star and sea urchin, i.e., ophiopluteus and echinopluteus (ICES, 1964), larvae was not possible due to limitations in the optical resolution of the VPR images. However, the majority of identifiable pluteus larvae originated from brittle stars, which are typical species of sand bottom habitats. Brittle stars, especially *Ophiura albida,* are known to be opportunistic species that are able to rapidly increase their abundance after disturbances, like cold winters (Neumann et al., 2009), and occur in extremely high densities in the more coastal areas of the southern German Bight (Reiss and Kröncke, 2004, Gutow et al., 2014). It is not known whether brittle stars inhabited the two OWF areas or surrounding regions in high densities at the time of our survey, as we do not have data or images from the sea bottom. However, in the year 2000 Callaway et al. (2002) found brittle stars at several 2 m beam trawl stations within a 50 km radius of the two OWFs. It may be that the soft bottom predatory and scavenging brittle stars indirectly benefitted from

the increased production at the foundations and reacted with a population increase. Whether the hard substrate benthic community also benefits from a locally increased pelagic primary and secondary production remains an open research task and depends, e.g., on the residence times of the water bodies inside the OWFs (Carpenter et al., 2016).
The high counts of pluteus larvae fit within the natural corridor of variability. In August 1983 Krause et al. (1986) observed a distinct high density patch of echinoderm larvae (33 Nl^{-1}) in the surface layer of a thermal front in the German Bight. This compares well with our observed maximum of 35 (Nl^{-1}) pluteus larvae. Krause et al. (1986) interpreted their result as an accumulation of non-motile organisms due to front-induced upwelling and convergent flows, as generally zooplankton of the Southern North Sea Water in the outer German Bight are dominated at that time of the survey by copepods (90%).
Some other plankton taxa like pilidium larvae of nemertean worms or polychaeta (Pectinariidae) larvae showed distinct relationships with hydrography, but were not affected by the presence of an OWF. Late ophiuroidea, brittle star, and larvae in their settlement phase were found in the deep waters within and west of BARD (see Appendix). Whether this sand-habitat species benefits from locally increased pelagic production within the OWF remains to be investigated. High densities of marine snow never co-occurred with high densities of copepods points indirectly towards copepods feeding on or disrupting marine snow as described by Möller et al. (2012).

Fish
Another possible top-down predation effect may be the zone of very low copepod densities occurring around 6.1°E at the downstream side of large numbers of pelagic, planktivorous fish at the BARD EW transect (Fig. 12). The high copepod density may be the cause of the unstructured spatial distribution of the planktivorous pelagic fish. There may not have been sufficient prey gradients to lead fish aggregations to areas with high food supply, given that copepods are the dominant prey organisms of clupeids in this region (Hardy, 1924, Last, 1989, Segers et al, 2007). However, if the highest pelagic fish abundances are found close to the turbine foundations, as observed by Schröder et al. (2013) and Krägefsky (2014), the hydroacoustic instruments under the vessel could not have detected this.

Conclusions & outlook

The survey provides empirical evidence that an OWF with 80 foundations decreases the summer water column stratification. This effect may also extend into its surrounding area by approximately half the diameter of an ambient tidal ellipse. Furthermore, there are indications that an OWF in a tidally affected stratified sea creates a *stirring effect*, with local upwelling cells at its lateral sides. However, the magnitude of the induced hydrodynamic processes may still fit into the corridor of natural variability leaving the quantification of cause-effect relationships a task for future studies and also for reshaped monitoring programs (Lindeboom et al., 2015). Nutrient supply to the depleted SML was enhanced in OWFs but a subsequent increase in phytoplankton biomass was not observed at the broader spatial scale of the wind farms. However, in one case increased phytoplankton and nutrient levels could be related to the residence time of water bodies within an OWF. Further, isolated pillars of high chlorophyll-*a* concentrations were found in and around the OWFs, and may be left over signatures of dissipated submesoscale features created by the turbine foundations. Given the ambient light levels, primary production below the thermocline can be expected to increase due to enhanced vertical mixing and a shallower and less intense stratification. In addition, increased nutrient influx into the surface layer will enhance surface layer primary production. The quantification of the increase in primary production, and whether the organic matter enhances the benthic or pelagic secondary production will be considered in future studies. High density patches of meroplankton observed at the boundaries of the OWFs point towards advantageous abiotic and biotic conditions for benthic species in the two OWFs. Based on our observations, pelagic fish distribution was not significantly affected by the OWFs, but this conclusion may have to be revised as the vertical echo sounder may not have detected fish close to the turbine foundations. Eventually, as many more OWFs will be in full operation in the near future, research should aim at the multi-disciplinary quantification of the wind wake effect on the regional ecosystem scale, with a focus on the cumulative effects of OWF clusters (Bergström et al, 2014) and on the trophic transfer of any increase in production. The discernment of OWF induced cause-effect relationships from natural variability remains a crucial challenge.

Acknowledgements

We thank the captain, R. Voss, and the crew of RV Heincke for their perfect support of our work. The two RV Heincke research cruises were supported by grant numbers AWI_HE429_00 and AWI_HE331_00. Further we thank T. Brüning (BSH) for the kind supply of BSHcmod current data and S. Kern (ICDC) for the MODIS data. Last not least we especially thank R. Kafemann (GTI) and C.-H. Hermanussen (BARD) for their invaluable support to obtain the permits to work inside the OWFs and the provision of the underwater images. We also thank the technicians and engineers of HZG and Hamburg University who operated and maintained the equipment and carried out lab work.

Contributions

Idea & Coordination: JF
Data analysis & interpretation: all
Manuscript writing: JF, CM, AT, RN
TRIAXUS data integration: AE, JF
CTD: TP, HL, RN
Nutrients: JvB, BW
VPR: KOM, DA, KH; SS
LOPC: MH, TD
Light: AE, OZ, JF
Particle drift: UC, JF
Stratification modelling: JC, JF
Hydroacoustic: DG, SJu
Zooscan: SJa
WP2: SE
HE331: RR

References

Backhaus, J., 1985. A Three-Dimensional Model for the Simulation of Shelf Sea Dynamics. Dt. hydrogr. Z. 38 (H 5): 167-262.

Becker, G. A., Dick, S., Dippner, J. W., 1992. Hydrography of the German Bight. Marine Ecology Progress Series, Vol. 91: 9-18

Bergström, L.; Kautsky, L.; Malm, T.; Rosenberg, R.; Wahlberg, M.; Capetillo, N.; Wilhelmsson, D., 2014. Effects of Offshore Wind Farms on Marine Wildlife - A Generalized Impact Assessment. Environmental Research Letters, 9, 1-12.

Broström, G., 2008. On the influence of large wind farms on the upper ocean circulation. Journal of Marine Systems 74, 585–591.

Bowers, D. G. and J. H. Simpson, 1987: Mean position of tidal fronts in European-shelf seas. Cont. Shelf Res., 7(1), 35–44.

BSH, 2013. Bundesamt für Seeschifffahrt und Hydrographie (BSH), Federal Maritime and Hydrographic Agency. Standard Investigation of the Impacts of Offshore Wind Turbines on the Marine Environment (StUK4) 87pp.

BSH, 2015. Bundesamt für Seeschifffahrt und Hydrographie (BSH), Federal Maritime and Hydrographic Agency. http://www.bsh.de/en/Marine_uses/Industry/Wind_farms/ (Accessed September 20, 2016).

Burson, A., M. Stomp, L. Akil, C. P. Brussaard, and J. Huisman. 2016. Unbalanced reduction of nutrient loads has created an offshore gradient from phosphorus to nitrogen limitation in the North Sea. Limnology and Oceanography, 61, 869-888.

Brzezinski, M. A. 1985. The Si:C:N ratio of marine diatoms: interspecific variability and the effect of some environmental variables. Journal of Phycology 21:347-357.

Callaway R, Alsvåg J, de Boois I, Cotter J, Ford A, Hinz H, Jennings S, Kröncke I, Lancaster J, Piet G, Prince P und Ehrich S., 2002. Diversity and community structure of epibenthic invertebrates and fish in the North Sea. ICES Journal of Marine Science, 59: 1199-1214.

Callies U, Plüß A, Kappenberg J, Kapitza H, 2011. Particle tracking in the vicinity of Helgoland, North Sea: a model comparison. Ocean Dyn 61, 2121-2139.

Callies, U., Gaslikova, L., Kapitza, H., Scharfe, M., 2016. German Bight residual current variability on a daily basis: principal components of multi-decadal barotropic simulations. Geo-Marine Letters, 1-12. doi:10.1007/s00367-016-0466-2

Carpenter JR, Merckelbach L, Callies U, Clark S, Gaslikova L, Baschek B., 2016. Potential Impacts of Offshore Wind Farms on North Sea Stratification. PLoS ONE 11(8): e0160830. doi:10.1371/journal.pone.0160830

Casulli V, Stelling GS, 1998. Numerical simulation of 3D quasi-hydrostatic, free-surface flows. J Hydraul Eng, 124, 678-686.

Cazenave, P.; Torres, R.; Allen, J., 2016. Unstructured Grid Modelling of Offshore Wind Farm Impacts on Seasonally Stratified Shelf Seas. Progress in Oceanography, 145, 25-41.

Clark, S.; Schroeder, F.; Baschek, B., 2014. The Influence of Large Offshore Wind Farms on the North Sea and Baltic Sea - A Comprehensive Literature Review. HZG Report 2014-6, pp 46.

Corbetta, G., Mbistrova, A., Ho, A., Pineda,I.,Ruby, K., 2016. Wind in power: 2015 European statistics. Report. European Wind Energy Association (EWEA), February 2016, 1-14.

Dick, S., Kleine, E., Müller-Navarra, S.H., Klein, H. and Komo, H., 2001: The Operational Circulation Model of BSH (BSHcmod)- Model description and validation. Berichte des Bundesamtes für Seeschifffahrt und Hydrographie, Nr. 29/2001, 49pp.

Dortch, Q. 1990. The interaction between ammonium and nitrate uptake in phytoplankton. Marine ecology progress series 61:183-201.

Gaslikova L, Weisse R, 2013. coastDat-2 TRIM-NP-2d Tide-Surge North Sea. World Data Center for Climate (WDCC) at DKRZ. doi:10.1594/WDCC/coastDat-2_TRIM-NP-2d

EEG, 2014: Erneuerbare-Energien-Gesetz vom 21. Juli 2014 (BGBl. I S. 1066)

Fernandes P. G., Korneliussen R. J., Lebourges-Dhaussy A., Masse J., Iglesias M., Diner N., Ona E., et al. 2006. Final Report to the EC, Q5RS-2001–02054; 2006. The SIMFAMI Project: Species Identification Methods from Acoustic Multifrequency Information.

Gasparini, S. and Antajan, E. 2013. PLANKTON IDENTIFIER: a software for automatic recognition of planktonic organisms. http://www.obs-vlfr.fr/~gaspari/Plankton_Identifier/index.php

Grasshoff, K., M. Erhardt, and K. Kremling. 1983. Methods of Seawater Analysis. 2nd Edition, 419 pp. Weinheim/Deerfield Beach, Florida: Verlag Chemie

Grashorn, S., Stanev, E. V., 2016.Kármán vortex and turbulent wake generation by wind park piles. Ocean Dynamics 66:1543–1557

Große, F., Greenwood, N., Kreus, M., Lenhart, H.-J., Machoczek, D., Pätsch, J., Salt, L., and Thomas, H., 2016. Looking beyond stratification: a model-based analysis of the biological drivers of oxygen deficiency in the North Sea, Biogeosciences, 13, 2511-2535, doi:10.5194/bg-13-2511-2016

Gorsky, G., M. D. Ohman, M. Picheral, S. Gasparini, L. Stemmann, J.-P. Romagnan, A. Cawood, S. Pesant, C. García-Comas, and F. Prejger, 2010. Digital zooplankton image analysis using the ZooScan integrated system. J. Plankton Res. (2010) 32 (3): 285-303 doi:10.1093/plankt/fbp124

Gutow, L. , Teschke, K. , Schmidt, A. , Dannheim, J. , Krone, R. and Gusky, M. , 2014. Rapid increase of benthic structural and functional diversity at the alpha ventus offshore test site. In: Ecological Research at the Offshore Windfarm alpha ventus - Challenges, Results and Perspectives, Wiesbaden, Springer Spektrum, pp 67-81, ISBN: 978-3-658-02461-1 . doi: 10.1007/978-3-658-02462-8_9

Hardy A. C., 1924. Fishery Investigations. Volume 7.(3). The herring in relation to its animate environment Part 1; p. 140. (Series 2).

Hill, A.E., I. D. James, P. F. Linden, J. P. Matthews, D. Prandle, J. H. Simpson, E. M. Gmitrowicz, D. A. Smeed, K. M. M. Lwiza, R. Durazo, A. D. Fox, D. G. Bowers and M. Weydert, 1993. Dynamics of Tidal Mixing Fronts in the North Sea [and Discussion]. Philosophical Transactions: Physical Sciences and Engineering, Vol. 343, No. 1669, Understanding the North Sea System (Jun. 15, 1993), pp. 431-446

Hijmans, R., J. and Jacob van Etten. 2012. raster: Geographic analysis and modelling with raster data. R package version 2.0-12. http://CRAN.R-project.org/package=raster

Holt, J., Umlauf, L., 2008. Modelling the tidal mixing fronts and seasonal stratification of the Northwest European Continental shelf, Continental Shelf Research, Vol 28, Issue 7, Pages 887-903

Hu Q, and Davis CS., 2006. Accurate automatic quantification of taxa-specific plankton abundance using dual classification with correction. Mar Ecol Prog Ser 306: 51−61

Huthnance, J. M., 1991. Physical Oceanography of the North Sea. Ocean Shoreline Managment 1991, 16, 199–231

ICES, 1964. Zooplankton Sheet 105 - ECHINODERMATA : LARVAE, Classes : Ophiuroidea and Echinoidea (PLUTEI), BY S. R. GEIGER), CONSEIL INTERNATIONAL POUR L'EXPLORATION DE LA MER, 5pp.

Kapitza H, 2008. MOPS – a morphodynamical prediction system on cluster computers. In: Laginha JM, Palma M, Amestoy PR, Dayde M, Mattoso M, Lopez JC (eds.) High Performance Computing for Computational Science –VECPAR 2008. June 2008, Toulouse, France. Springer, Heidelberg, pp 63-68

Kèrouel, R., and A. Aminot. 1997. Fluorometric determination of ammonia in sea and estuarine waters by direct segmented flow analysis. Marine Chemistry 57:265 - 275.

Kirk, J. T. 0. ,1994. Light and photosynthesis in aquatic ecosystems. Cambridge Univ. Press, Cam- bridge UK. 509 pp.

Krause, G. , Gerdes, D. , Schaumann, K. , Hesse, K. and Budéus, G., 1986. Frontal systems in the German Bight and their physical and biological effects , In: J.C.J. Nihoul, (Ed) Elsevier, Marine interfaces ecohydrodynamics, pp 119-140 Amsterdam .

Krägefsky, S., 2014. Effects of the alpha ventus offshore test site on pelagic fish. In: BSH and BMU, 2014. Ecological Research at the Offshore Windfarm alpha ventus - Challenges, Results and Perspectives. Federal Maritime and Hydrographic Agency (BSH), Federal Ministry for the Environment, Nature Conservation and Nuclear Safety (BMU). Springer Spektrum. 201 pp. Eds: A. Beiersdorf, A. Radecke.

Krone, R., L. Gutow, T. J. Joschko & A. Schroder, 2013. Epifauna dynamics at an offshore foundation—Implications of future wind power farming in the North Sea. Marine Environmental Research 85: 1–12.

Lass, H.U., Mohrholz, V. Knoll, M., Prandke, H., 2008. Enhanced mixing downstream of a pile in an estuarine flow, Journal of Marine Systems 74, 505-527.

Last J. M., 1989. The food of herring, Clupea harengus, in the North Sea, 1983–1986. Journal of Fish Biology 1989; 34:489-501.

Lee, A. L., 1980. Chapter 14 North Sea: Physical Oceanography. In: Elsevier Oceanography Series Volume 24, Part B, F.T. Banner, M.B. Collins, K.S. Massie (Eds.), The North-West European Shelf Seas: The Sea Bed and the Sea in Motion, Vol. II, Elsevier, Amsterdam, pp. 467–493

Li, X., Chi, L., Chen, X., Ren, Y., Lehner, S., 2014. SAR observation and numerical modelling of tidal current wakes at the East China Sea offshore wind farm. Journal of Geophysical Research: Oceans 119 (8), 4958–4971.

Lindeboom, H. J. , Degraer, S. , Dannheim, J. , Gill, A. B. and Wilhelmsson, D., 2015. Offshore wind park monitoring programmes, lessons learned and recommendations for the future , Hydrobiologia . doi: 10.1007/s10750-015-2267-4

Ludewig, E., 2015. On the Effect of Offshore Wind Farms on the Atmosphere and Ocean Dynamics
Series: Hamburg Studies on Maritime Affairs, Vol. 31, 162pp. Springer International Publishing Switzerland, DOI 10.1007/978-3-319-08641-5

Möller, K. O., St. John, M., Temming, A., Floeter, J., Sell, A. F., Herrmann, J.-P. and Möllmann, C., 2012. Marine snow, zooplankton and thin layers: indications of a trophic link from small-scale sampling with the Video Plankton Recorder. Mar. Ecol. Prog. Ser., 468, 57–69.

Möller,K.O., J.O. Schmidt, M. St.John, A. Temming, R. Diekmann, J. Peters, J. Floeter, A.F. Sell, J.-P. Herrmann, C. Möllmann. “Effects of climate-induced habitat changes on a key zooplankton species”. Journal of Plankton Research 37 (3). (2015): S. 530-541. doi: 10.1093/plankt/fbv033

Neumann, H., Reiss, H., Rakers, S., Ehrich, S., and Kröncke, I., 2009. Temporal variability in southern North Sea epifauna communities after the cold winter of 1995/1996. – ICES Journal of Marine Science, 66: 2233–2243.

Nerge,P., Lenhart, H., 2010. Wake Effects In Analyzing Coastal and Marine Changes: Offshore Wind Farming as a Case Study. Zukunft Küste - Coastal Futures Synthesis Report. (M. Lange, B. Burkhard, S. Garthe, K. Gee, A. Kannen, H. Lenhart, W. Windhorst), Series: No. 36, Chapters: 5.3, pp. 68–73, LOICZ Research and Studies (GKSS Research Center, Geesthacht, Germany), 2010

North, R.P., R. Riethmüller, and B. Baschek, 2016. Detecting small–scale horizontal gradients in the upper ocean using wavelet analysis. Estuarine, Coastal and Shelf Science. 180: 221–229. DOI:10.1016/j.ecss.2016.06.03

NSTF, North Sea Task Force, 1993. North Sea Quality Status Report 1993. Oslo and Paris Commissions, London. Olsen and Olsen, Fredensborg, Denmark. 132 pp.

Paskyabi, B. M., Fer, I. , Jenkins, A.D., 2012. Surface gravity wave effects on the upper ocean boundary layer: Modification of a one-dimensional vertical mixing model. Continental Shelf Research, Volume 38, 63-78

Paskyabi, B. M., Fer, I., 2012. Upper Ocean Response to Large Wind Farm Effect in the Presence of Surface Gravity Waves. Energy Procedia 24, 245 – 254.

Pineda, I., Ruby, K., 2016. The European offshore wind industry. Key trends and statistics 1st half 2016. 19pp, WindEurope asbl/vzw, Rue d’Arlon 80, B-1040 Brussels, Belgium, www.windeurope.org

Pohlmann, T., 1996. Predicting the thermocline in a circulation model of the North Sea. Part I: Model description, calibration, and verification. Continental Shelf Research 7: 131-146.

Pohlmann, T., 2006. A meso-scale model of the central and southern North Sea: Consequences of an improved resolution. Continental Shelf Research 26: 2367-2385.

Queste, B. Y., Fernand, L., Jickells, T. D., Heywood, K. J., and Hind, A. J., 2016. Drivers of summer oxygen depletion in the central North Sea, Biogeosciences, 13, 1209-1222, doi:10.5194/bg-13-1209-2016

R Core Team (2015). R: A language and environment for statistical computing. R Foundation for Statistical Computing, Vienna, Austria. URL http://www.R-project.org/.

Reiss, H. and Kröncke I., 2004. Seasonal variability of epibenthic communities in different areas of the southern North Sea. ICES Journal of Marine Science, 61: 882-905.

Rennau H, Schimmels S, Burchard H., 2012. On the effect of structure-induced resistance and mixing on inflows into the Baltic Sea: A numerical study. Coastal Eng. 2012; 60:53–68.

Segers, F. H. I. D, Dickey-Collas, M., and Rijnsdorp, A. D., 2007. Prey selection by North Sea herring (*Clupea harengus*), with special reference to fish eggs. ICES Journal of Marine Science, 64: 60–68.

Simpson, J.H., 1981. The Shelf-Sea Fronts: Implications of their Existence and Behaviour. Phil. Trans. R. Soc. Lond. A. 302, 531-546.

Simpson, J.H. , P.B. Tett, M.L. Argote-Espinoza, A. Edwards, K.J. Jones, G. Savidge, 1982. Mixing and phytoplankton growth around an island in a stratified sea, Continental Shelf Research, Volume 1, Issue 1, Pages 15-31, ISSN 0278-4343, http://dx.doi.org/10.1016/0278-4343(82)90030-9.

Schlitzer, R., Ocean Data View, odv.awi.de, 2016

Schröder, A. , Gutow, L. , Joschko, T. , Krone, R. , Gusky, M. , Paster, M. and Potthoff, M., 2013. Benthosökologische Auswirkungen von Offshore-Windeneregieparks in der Nordsee (BeoFINO II). Abschlussbericht zum Teilprojekt B „Benthosökologische Auswirkungen von Offshore-Windenergie-parks in Nord- und Ostsee. Prozesse im Nahbereich der Piles“, (BMU Förderkennzeichen 0329974B). hdl:10013/epic.40661.d001

Schrum,C., 1997. Thermohaline stratification and instabilities at tidal mixing fronts: results of an eddy resolving model for the German Bight, Continental Shelf Research, Volume 17, Issue 6, 1997, Pages 689-716,

Thyng, K.M., C.A. Greene, R.D. Hetland, H.M. Zimmerle, and S.F. DiMarco. 2016. True colours of oceanography: Guidelines for effective and accurate colourmap selection. Oceanography 29(3):9–13, http://dx.doi.org/10.5670/oceanog.2016.66.

Topcu, D., Behrendt, H., Brockmann, U., Claussen, U., 2011. Natural background concentrations of nutrients in the German Bight area (North Sea). Environ Monit Assess, Vol 174 / 1: 361-388

Topcu, H. D. and Brockmann, U. H., 2015. Seasonal oxygen depletion in the North Sea, a review, Mar. Pollut. Bull., 99, 5–27. doi:10.1016/j.marpolbul.2015.06.021

Troupin, C., Barth, A., Sirjacobs, D., Ouberdous, M., Brankart, J.-M., Brasseur, P., Rixen, M., Alvera Azcarate, A., Belounis, M., Capet, A., Lenartz, F., Toussaint, M.-E., & Beckers, J.-M., 2012. Generation of analysis and consistent error fields using the Data Interpolating Variational Analysis (Diva). Ocean Modelling, 52-53, 90-101.

van der Molen J, Smith HCM, Lepper P, Limpenny S, Rees J., 2014. Predicting the large-scale consequences of offshore wind turbine array development on a North Sea ecosystem. Cont Shelf Res. 85:60–72. doi: 10.1016/j.csr.2014.05.018

Vanhellemont, Q., Ruddick, K., 2014. Turbid wakes associated with offshore wind turbines observed with Landsat 8. Remote Sensing of Environment 145, 105-115.

van Leeuwen, S., P. Tett, D. Mills, and J. van der Molen, 2015. Stratified and nonstratified areas in the North Sea: Long-term variability and biological and policy implications, J. Geophys. Res. Oceans, 120, 4670–4686, doi:10.1002/2014JC010485.

Wickham, H., 2011. The Split-Apply-Combine Strategy for Data Analysis. Journal of Statistic al Software, 40(1), 1-29. URL http://www.jstatsoft.org/v40/i01/.

Zielinski O, Oschlies A, Llinas O, Reuter R (2002) Underwater light field parameterization an d its effecton a one-dimensional ecosystem model at station ESTOC, north of the Canary Isla nds. Deep-Sea Research II 49 (17), 3529-3542.